GULF STREAM VELOCITY STRUCTURE THROUGH COMBINED INVERSION OF HYDROGRAPHIC AND ACOUSTIC DOPPLER DATA

by

STEPHEN D. PIERCE

B.S.E.E., Tufts University
(1984)

SUBMITTED TO THE DEPARTMENT OF EARTH,
ATMOSPHERIC AND PLANETARY SCIENCES
IN PARTIAL FULFILLMENT OF
THE REQUIREMENTS FOR THE
DEGREE OF

MASTER OF SCIENCE IN
PHYSICAL OCEANOGRAPHY

at the

MASSACHUSETTS INSTITUTE OF TECHNOLOGY

October 1986

Signature of Author_____
Department of Earth, Atmospheric and Planetary Sciences

Certified by_____
Terrence M. Joyce
Thesis Supervisor

Accepted by_____
W. F. Brace
Chairman, Departmental Graduate Committee

GULF STREAM VELOCITY STRUCTURE THROUGH COMBINED INVERSION OF HYDROGRAPHIC AND ACOUSTIC DOPPLER DATA

by

STEPHEN D. PIERCE

Submitted to the Department of Earth,
Atmospheric, and Planetary Sciences
on October 1, 1986 in partial fulfillment of the
requirements for the Degree of Master of Science in
Physical Oceanography

ABSTRACT

Near-surface velocities from an acoustic doppler instrument are used in conjunction with CTD/O_2 data to produce estimates of the absolute flow field off of Cape Hatteras. The data set consists of two transects across the Gulf Stream made by the R/V Endeavor cruise EN88 in August 1982. An inverse procedure is applied which makes use of both the acoustic doppler data and property conservation constraints. Velocity sections at approximately 73°W and 71°W are presented with formal errors of 1-2 cm/s. The net Gulf Stream transports are estimated to be 116 ± 2 Sv across the 'south' leg and 161 ± 4 Sv across the 'north'. A Deep Western Boundary Current transport of 4 ± 1 Sv is also estimated. While these values do not necessarily represent the mean, they are accurate estimates of the synoptic flow field in the region.

1. Introduction

The determination of absolute velocity fields from hydrographic data leads to the familiar problem of how to reference the geostrophic calculations. Historically this reference velocity problem has been solved by a somewhat arbitrary choice of a level of no motion. This assumption has been made simply out of necessity due to the scarcity of good direct velocity measurements. For a high velocity region such as the Gulf Stream, the level of no motion assumption can be an especially poor one. Attempts have been made to get a better estimate of the absolute velocities and transports in the Gulf Stream through the use of neutrally buoyant floats (eg. Volkmann, 1962), discrete current meters (eg. Richardson, 1977), or shipborne transport measurements (Halkin and Rossby, 1985). An inherent drawback with any of these methods is the relatively wide spacing of the current measurements which can lead to spatial aliasing. The acoustic doppler instrument used in the present study has the advantage of providing very dense spatial coverage of near-surface absolute velocities, eliminating this type of aliasing.

An innovative approach to the reference velocity problem making use of linear inverse theory was introduced by Wunsch (1978). This technique combines pure geostrophy with simple assumptions of conservation of mass and other properties within a certain volume of the ocean. The geostrophic inversion method offers a formal and objective technique for determining absolute velocities when only hydrographic and property data are measured: the 'pure' hydrographic inversion. It has the capability, however, to easily incorporate any other data (eg. velocity data) that

might be available into the inverse calculation. The problem will typically be an underdetermined one; a principle of maximum simplicity is used to choose the best estimate from the range of possible solutions.

As part of the study of warm core ring 82B off of Cape Hatteras, two transects were made from the Slope Water, across the Gulf Stream, and well into the Sargasso Sea. On 20-25 August 1982, the R/V Endeavor was used to obtain these two series of CTD/O_2 stations at approximately 73°W and 71°W (fig. 1). These sections were occupied to identify the water mass characteristics of the 'undisturbed' regions on either side of ring 82B (Olson et al., 1985). Simultaneous with the collection of hydrographic data, a shipborne acoustic doppler instrument measured absolute current velocities near the surface (Joyce, Bitterman, and Prada, 1982).

This data set provides the tempting opportunity to use the acoustic doppler velocities as a reference for geostrophic calculations, yielding a complete picture of the circulation in the region. The errors in the velocities and transports associated with this direct method prove to be substantial, however. The convenient geometry of the transects allows transport budgeting constraints to be imposed, suggesting the use of a pure geostrophic inversion (Wunsch, 1978). These constraints are used in combination with the measured velocities to yield a more accurate absolute flow field.

This combined inversion technique was first used by Joyce, Wunsch, and Pierce (1986) who applied it to the EN86 data set from June 1982. The present study closely follows this work, applying a similar inversion

method to the EN88 data from August 1982. Figure 2 shows the positions of both the EN86 and EN88 transects; they are quite similar, although the EN86 sections do not extend as far on the Sargasso Sea side. The successful use of these methods with the EN86 data set helped motivate the application to the EN88 case. In both cases, the combined inversion technique makes use of all of the available information about the system, both the CTD/O_2 and the acoustic doppler data, to produce the best possible estimate of the circulation in the region.

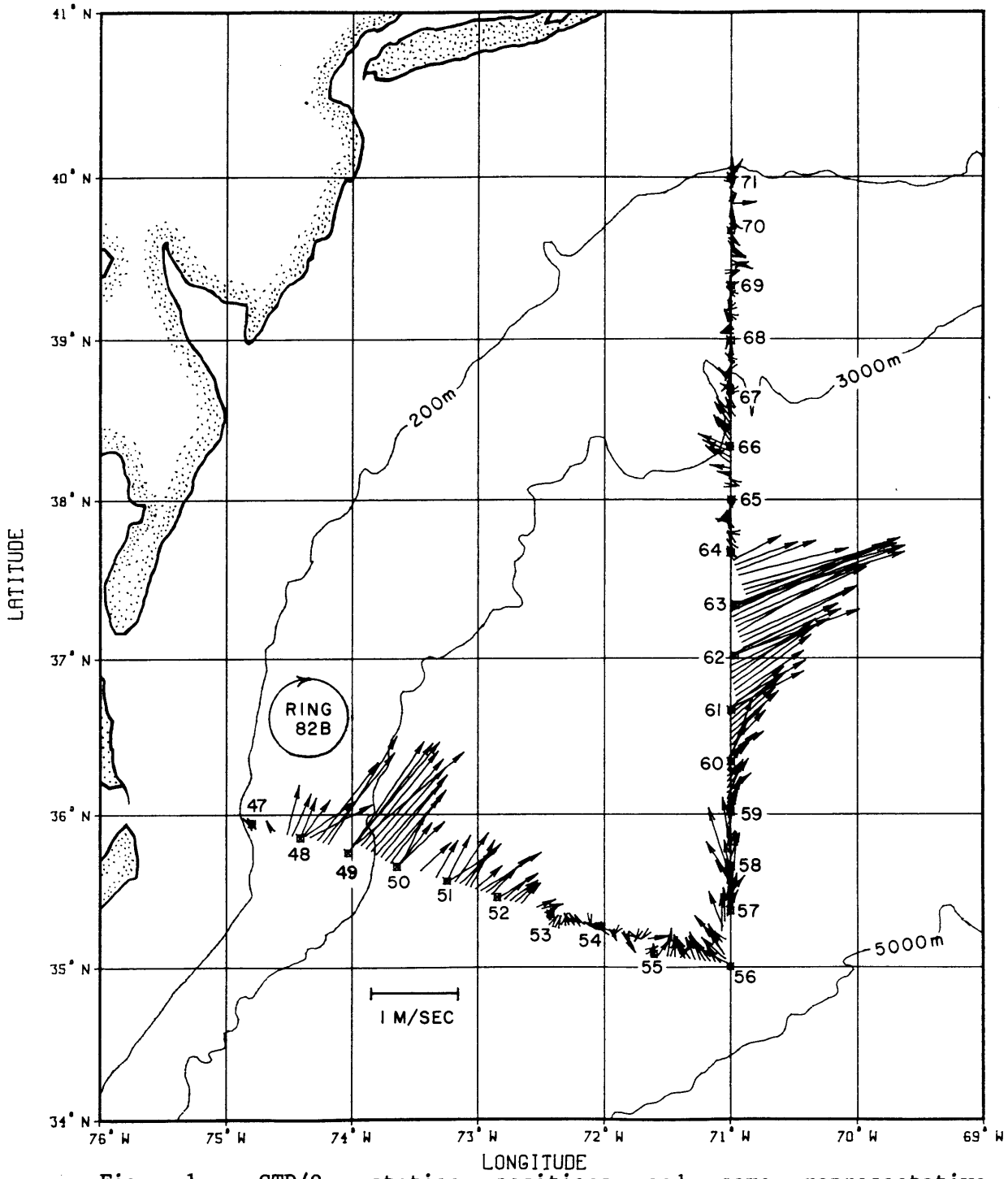

Fig. 1. CTD/O_2 station positions and some representative acoustic doppler vectors from the 60 m depth bin. Approximate location of warm-core ring 82B is also indicated.

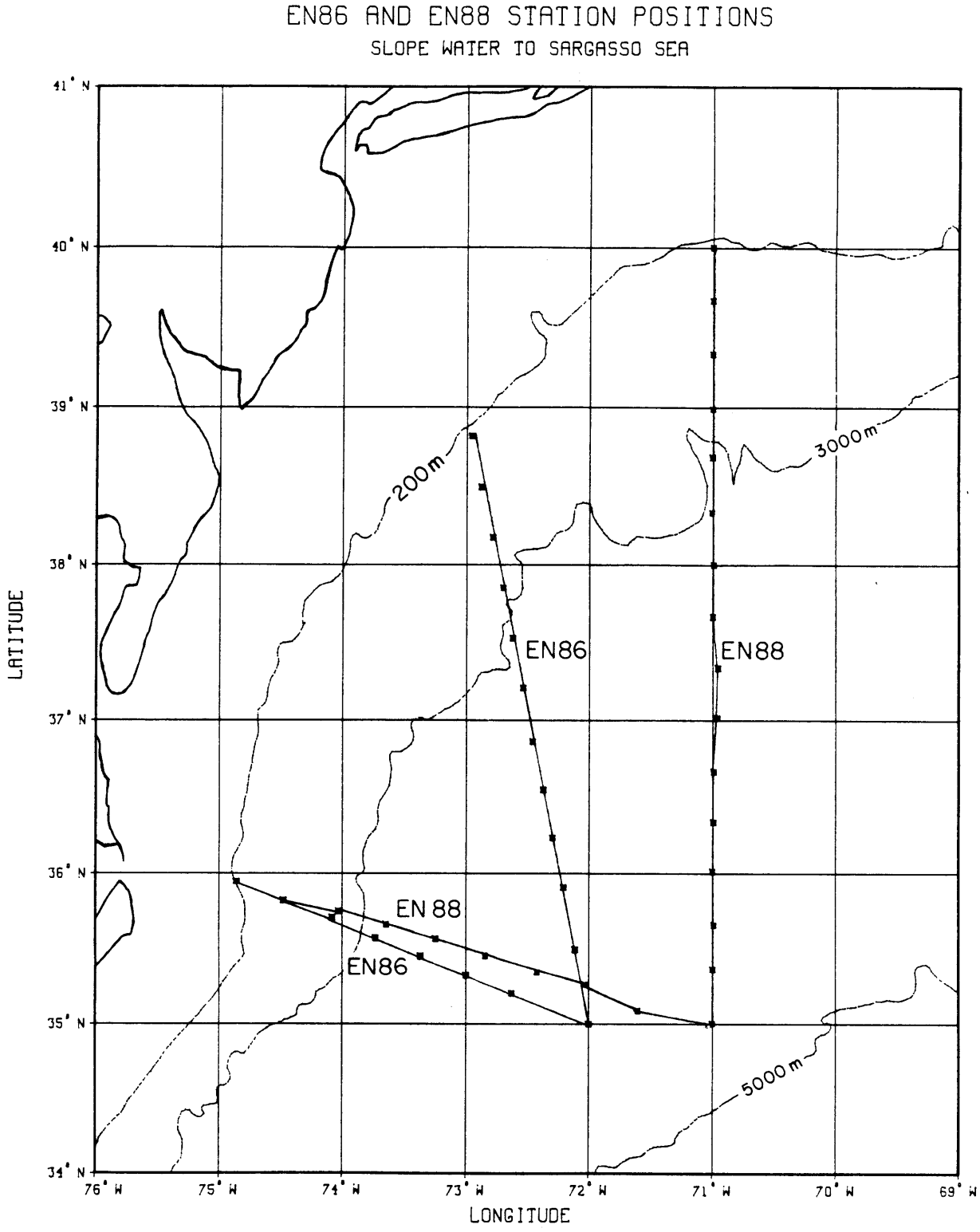

Fig. 2. The EN86 transects used by Joyce, Wunsch, & Pierce (1986) compared to the EN88 sections used in the present study.

2. Description of Data

A brief discussion of the operation of the acoustic doppler instrument is provided here; a full description of the system is given by Joyce et al. (1982). From the Ametek-Straza transducer mounted in the hull of the ship, a 300 kHz acoustic pulse is emitted every 1.2 seconds in four beams oriented fore, aft, port, and starboard, all 30° from vertical. The reflected signal is then received in a frequency-locked loop in 31 time intervals of 10 msec each. These intervals correspond to vertical depth averaging bins of 6.4 m thickness in the water column. From the doppler frequency shifts along the axes of each of the four beams, we can solve for the horizontal velocity components at each depth bin. The noise level inherent within the instrument yields a resolution of about ±1 cm/s for each raw doppler velocity.

An averaging interval of 10 minutes is chosen to reduce the presence of ship roll or heave in the raw velocity data. Each 10 minute value is the vector average of every 'good' velocity measured within that interval, where the return signal strength was above a certain threshold. While the nominal depth to which the acoustic signal penetrates is 150 m, the percentage of good data drops off rapidly below about 100 m. The data return also varies with the amount of scatterers (eg. plankton, temperature microstructure) present in the water column.

The shipborne doppler data must be added to an accurate ship velocity to yield absolute velocities relative to the earth. Ship velocity is found by differencing two positions separated in time, which depends upon precise navigation. The Northstar 6000 Loran receiver used is

found to have a noise level of ±0.1 μsec or ±30 m in ship location. Over the ten minute averaging time, this translates to a ship speed uncertainty of ±10 cm/s. Another source of error arises from the possible misalignment of the transducer mounting with the axis of the ship's gyro compass. If the ship is moving forward at a speed U, a small error $\delta\theta$ in the transducer angle will generate an apparent velocity perpendicular to the ship's path of size $U\sin\delta\theta$. This error ought to be systematic in nature once the instrument has been mounted in the ship; the offset will be either to the right or the left of the ship track. An angular error of 0.3° might be expected in the alignment. For a typical ship speed of 5 m/s, this produces an offset error of 2.6 cm/s in the athwartship velocity. A systematic error of approximately this size might therefore be expected.

The data set from Endeavor cruise EN88 consists of two sections of CTD/O_2 casts as well as the continuously measured 10 minute blocks of acoustic doppler velocities. The CTD data set was collected with an NBIS instrument and processed by the WHOI CTD group. Acoustic doppler velocities from four depth bins between 60 m and 99 m were ultimately used in the reference velocity calcalation. Data from depths shallower than this might be affected by the ageostrophic surface mixed layer, while below 100 m the quality of the data drops off sharply in most cases. Figure 1 shows some representative velocity vectors from the 60 m depth. Between each CTD station pair, the components of the vectors perpendicular to the station pair are averaged to yield a single normal velocity at a certain depth. These velocities are then integrated via the thermal wind to a

common depth, 100 db, and a vertical average weighted by the data return at each depth is performed. The resulting velocity picture is referenced by data at four different depths depending on how much data was available at each depth. As noted above, navigational uncertainty results in an estimated error of ±10 cm/s for each 10 minute doppler velocity. Between 10 and 15 of these go into the horizontal averaging to yield a single velocity between each station pair, reducing this presumably random error to approximately ±3 cm/s. This is the predicted noise level in the acoustic reference velocity for each station pair.

Throughout the discussion the section consisting of stations 47-56 will be known as the 'south' section and stations 56-71 as the 'north' section (fig. 1). Plots of potential temperature, salinity, oxygen, and potential density referenced to the surface appear in figs. 3 (south) and 4 (north). The Gulf Stream region is clearly identified by the strongly sloping isolines of all of the properties. The surface temperatures greater than 26°C and sub-surface salinity maximum (greater than 36.6 ppt) are both typical of the Gulf Stream at this time of year. In the Slope Water region to the north (stations 68-71, fig. 4), the intrusion of shelf and Slope water is identified by the inversions of temperature, salinity, and oxygen in the upper 100 m (Stalcup et al., 1985). At the Sargasso Sea corner of the triangular area (sta. 56, figs. 3 or 4), the Eighteen Degree Water has a thickness of approximately 175 m, defined by $\theta = 17.9 \pm 0.3$ °C and $S = 36.5 \pm 0.1$ ppt. An intriguing aspect of the Cape Hatteras region is the presence of the Deep Western Boundary Current (DWBC) and the nature of its crossing underneath

the Gulf Stream. The DWBC is identified in both the south and north sections by the oxygen maximum (>6.2 ml/l) at about 3400 m. These deep waters with high oxygen spread to the south and west, in opposition to the Gulf Stream.

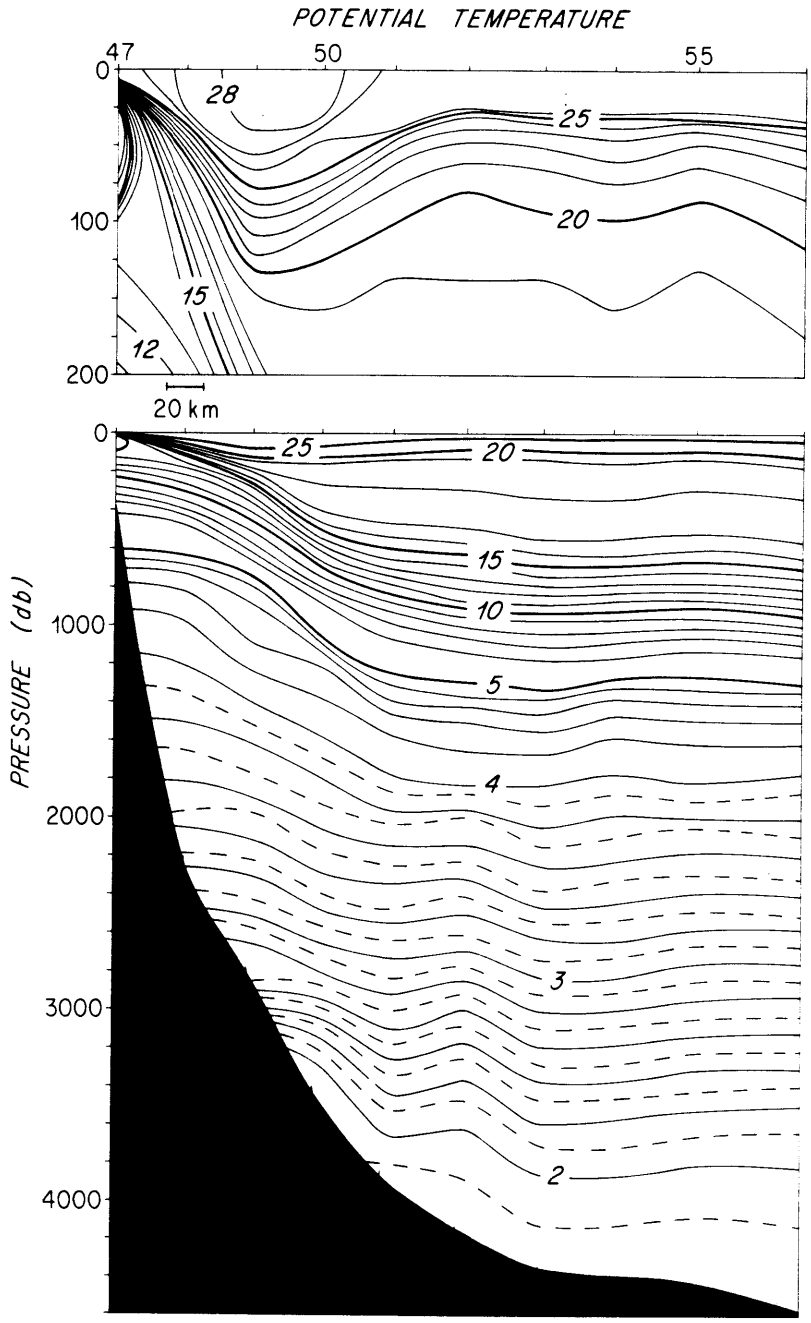

A.

Fig. 3a-d. Property distributions for the south section (approximately 73°W): potential temperature, salinity, O_2, and σ_θ. Vertical exaggeration is 50:1.

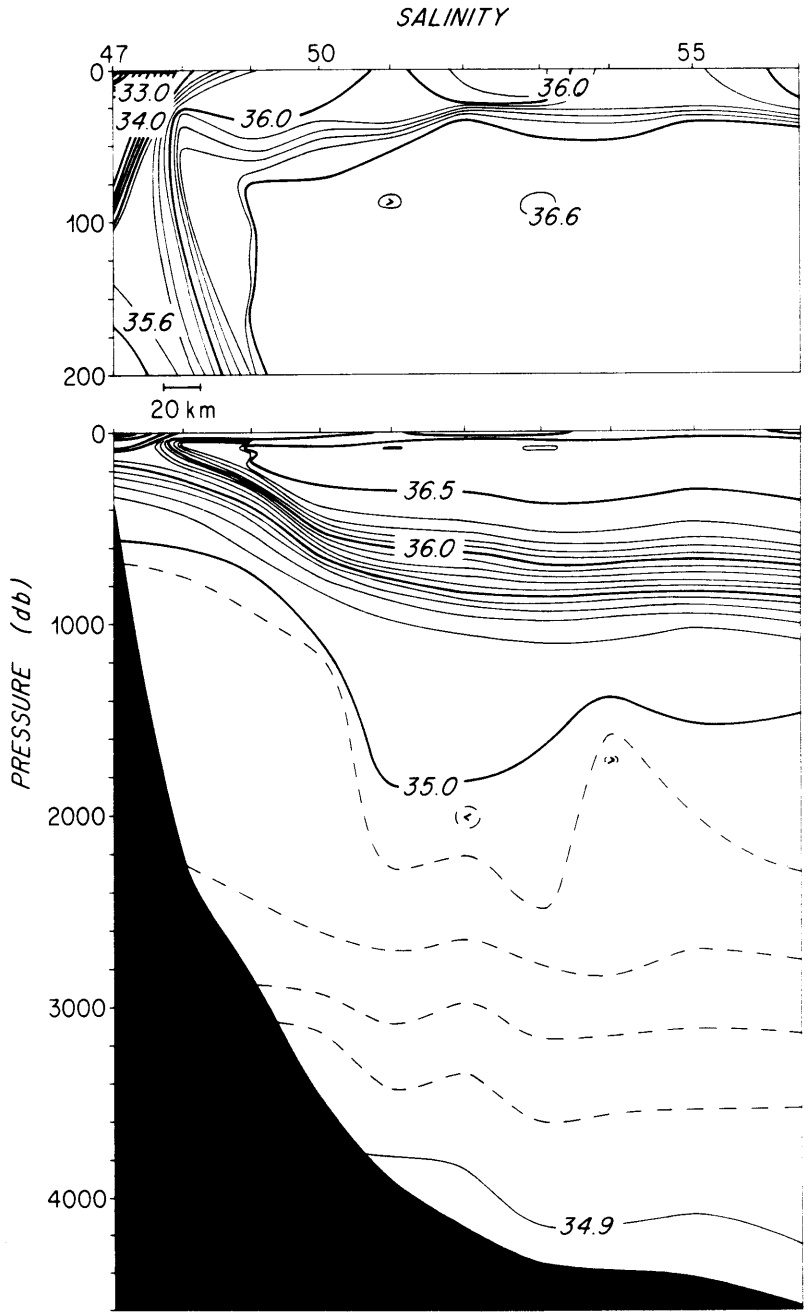
SALINITY
47
50
55
0
100
200
33.0
34.0
36.0
36.0
36.6
35.6
20 km
0
1000
2000
3000
4000
PRESSURE (db)
36.5
36.0
35.0
34.9

B.

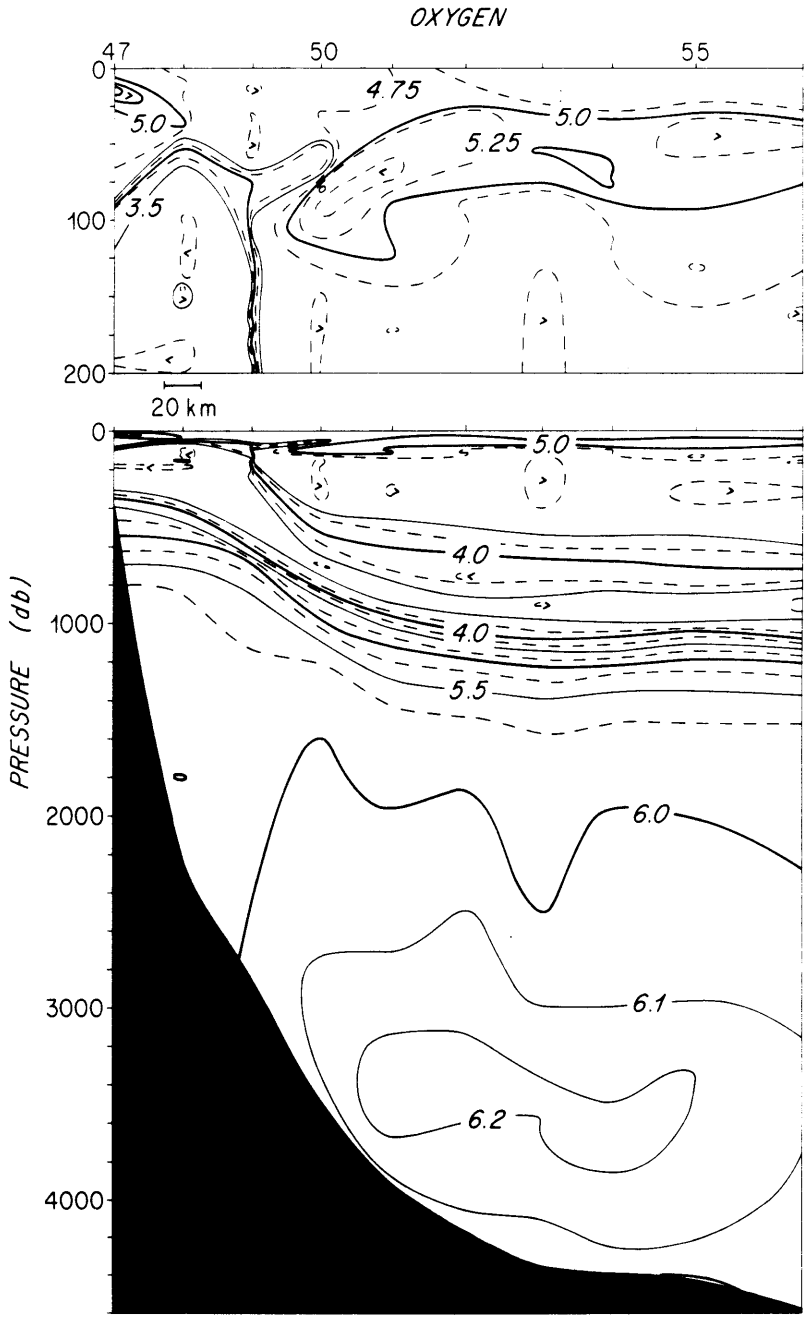
OXYGEN
47
50
55
0
100
200
4.75
5.0
5.0
5.25
3.5
20 km
0
5.0
4.0
4.0
5.5
1000
2000
3000
4000
6.0
6.1
6.2
PRESSURE (db)

C.

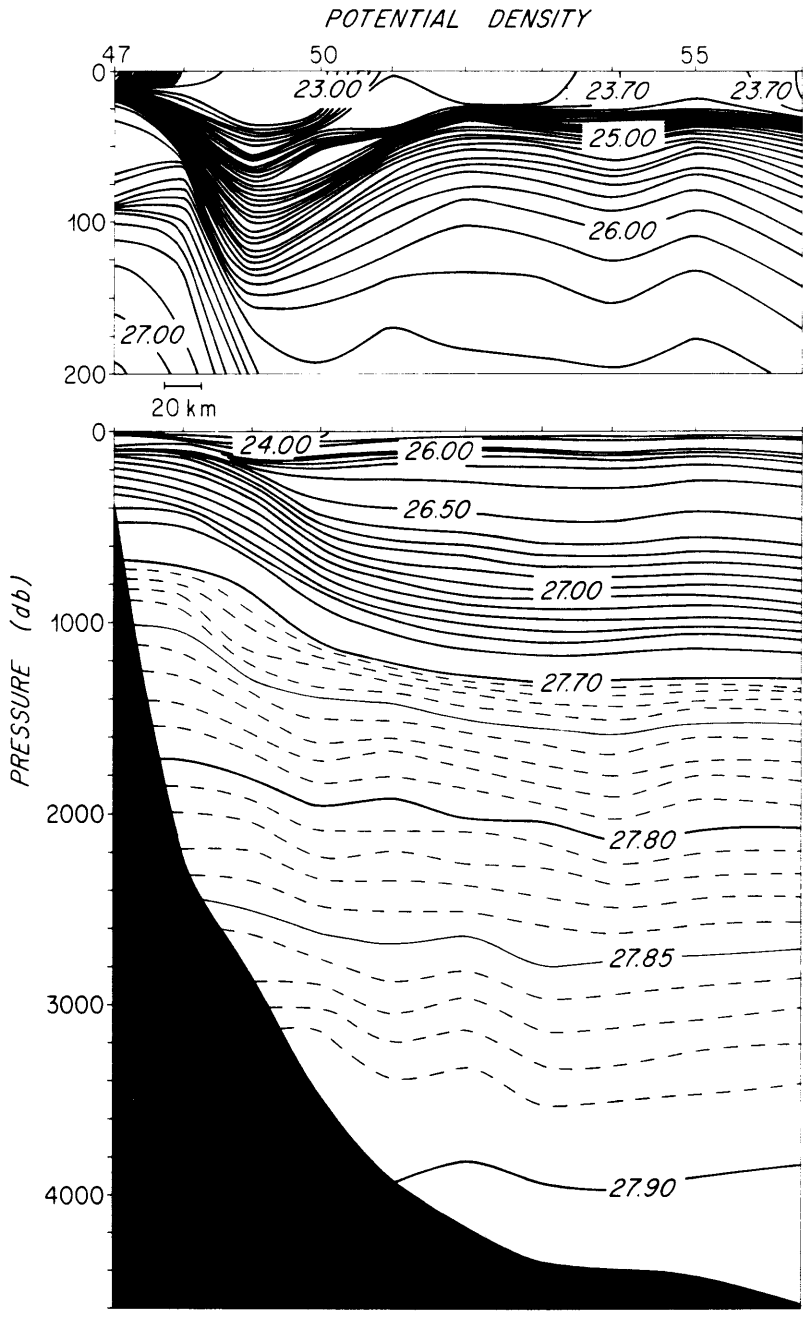
POTENTIAL DENSITY
47
50
55
0
100
200
23.00
23.70
23.70
25.00
26.00
27.00
20 km
0
1000
2000
3000
4000
PRESSURE (db)
24.00
26.00
26.50
27.00
27.70
27.80
27.85
27.90

D.

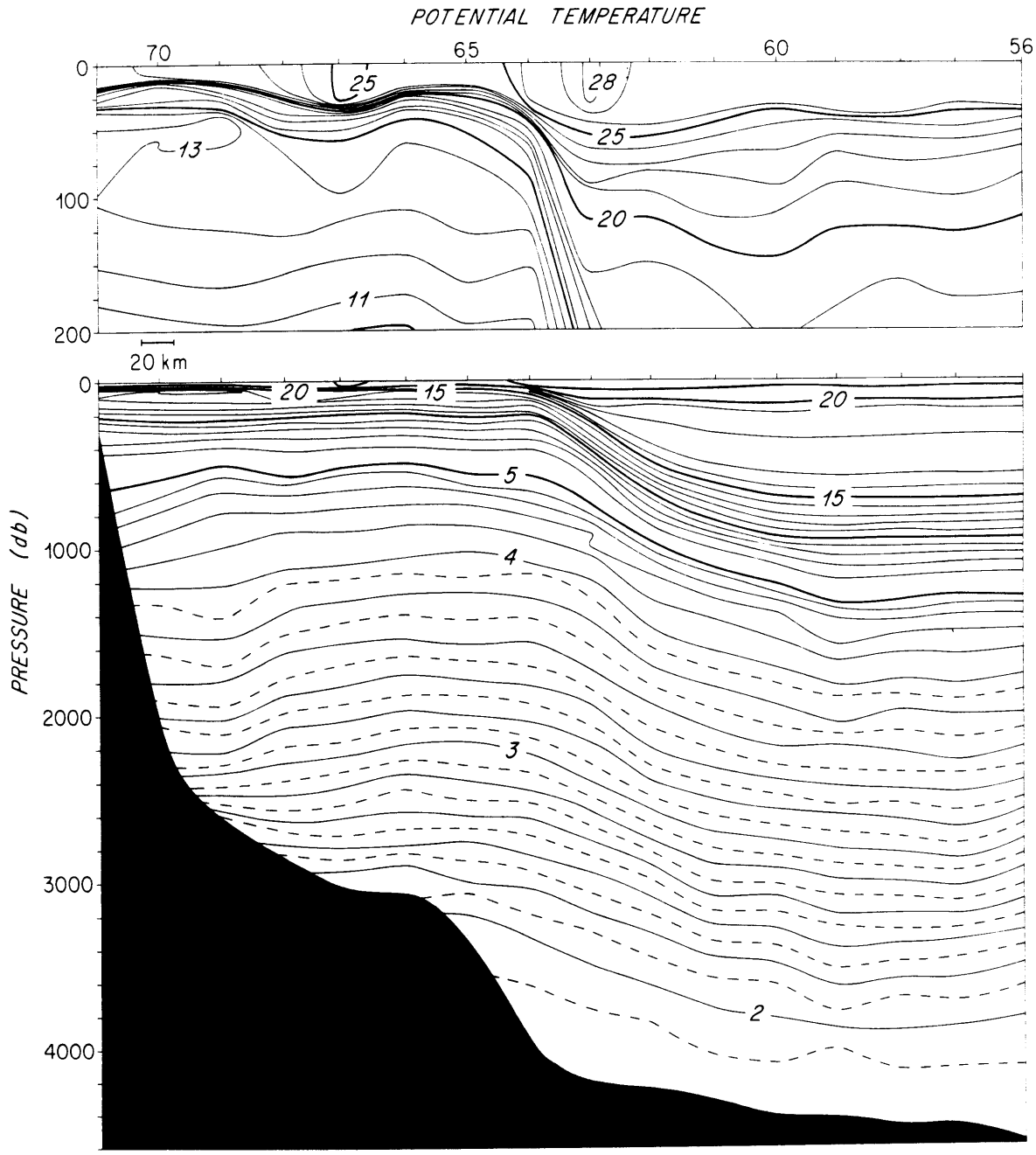

A.

Fig. 4a-d. Property distributions for the north section (on 71°W): potential temperature, salinity, O_2, and σ_θ.

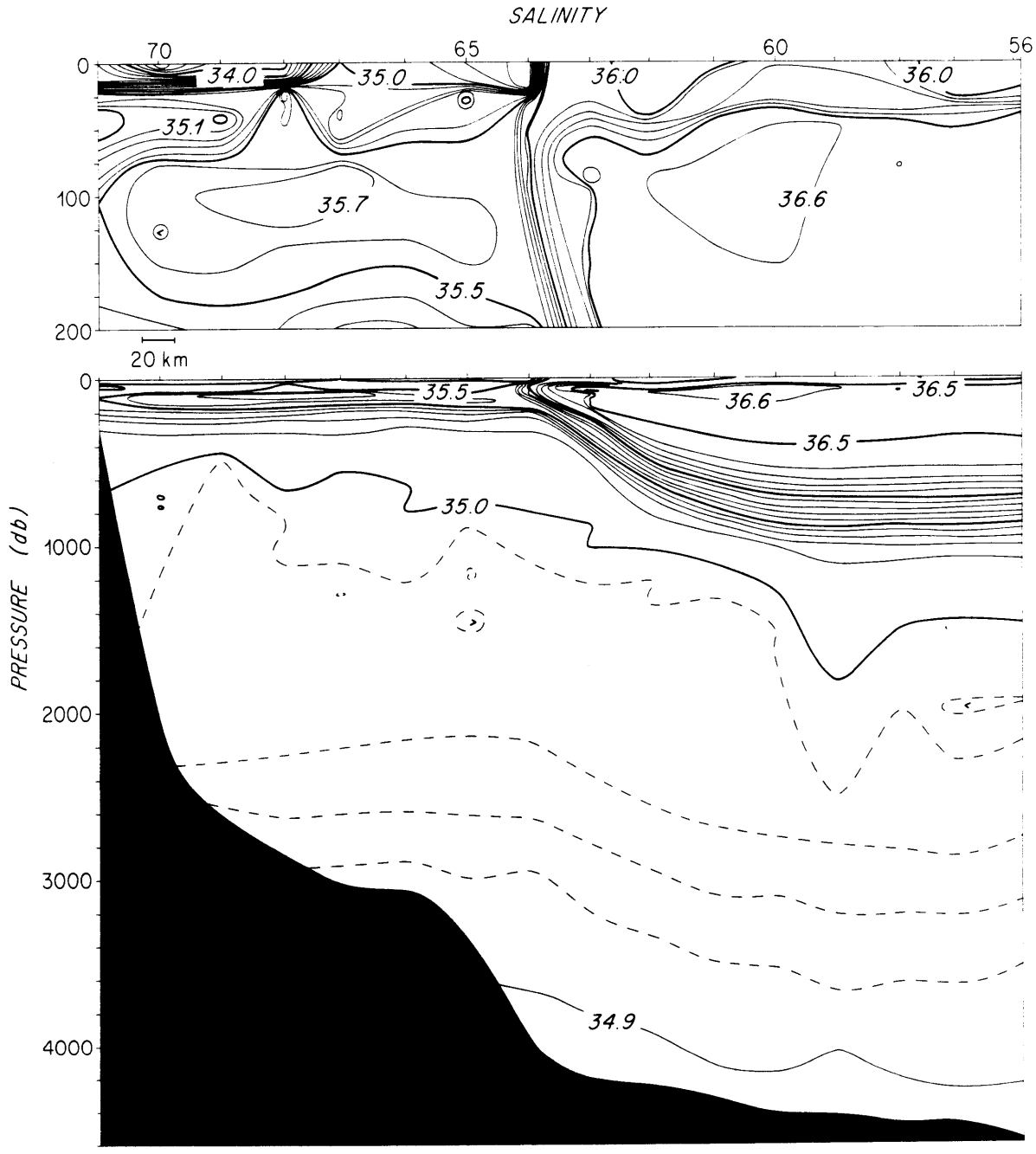
SALINITY
70
65
60
56
0
100
200
34.0
35.0
36.0
36.0
35.1
35.7
36.6
35.5
20 km
0
35.5
36.6
36.5
36.5
35.0
1000
2000
3000
4000
34.9
PRESSURE (db)

B.

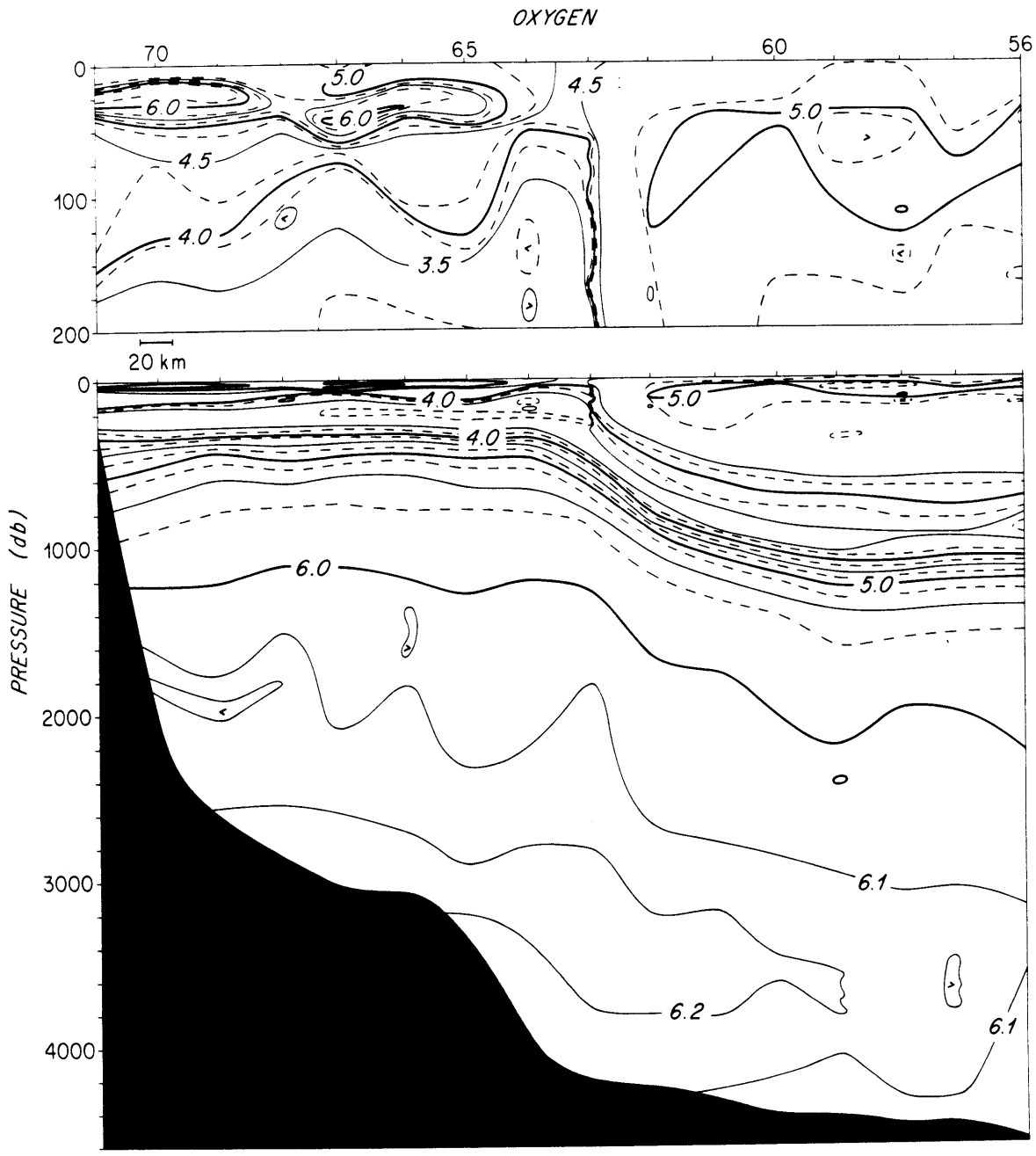
OXYGEN
70
65
60
56
0
100
200
5.0
6.0
6.0
4.5
4.5
4.0
3.5
5.0
0
20 km
0
1000
2000
3000
4000
PRESSURE (db)
4.0
4.0
5.0
6.0
5.0
6.1
6.2
6.1

c.

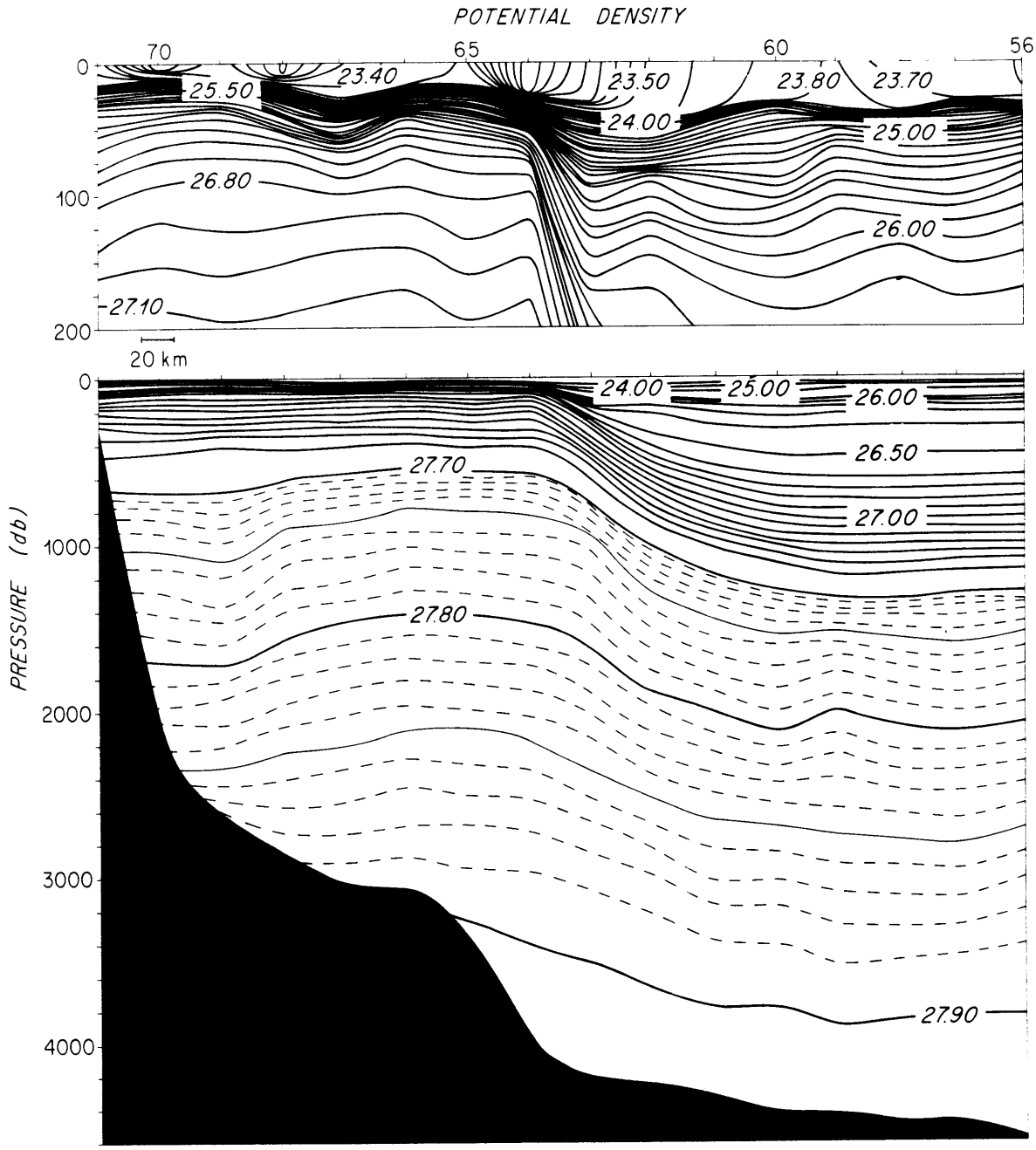
POTENTIAL DENSITY
70
65
60
56
0
100
200
25.50
23.40
23.50
23.80
23.70
24.00
25.00
26.80
26.00
27.10
20 km
0
1000
2000
3000
4000
PRESSURE (db)
24.00
25.00
26.00
26.50
27.70
27.00
27.80
27.90

D.

3. Absolute Velocity Estimation

The absolute velocity field across each of these sections will be estimated in two ways: direct use of the acoustic velocities to reference the geostrophic calculations, and the combined use of the acoustic velocities along with mass, salt, and O_2 conservation constraints. Both of these methods rely upon the assumption of pure geostrophy in this region. The acoustic doppler instrument might offer the possibility of testing this assumption directly, since it simultaneously measures velocities at different depths; the acoustic shear can be compared to the geostrophic shear. In this case, however, the reliable data only cover a depth range of 40 m, and the measured shears over such a small Δz are below our noise level. Better depth penetration of the doppler signal would be required for such a direct test of geostrophy.

Within our region the Gulf Stream takes a broad turn to the east; a centripetal acceleration term might become important in the cross-stream momentum balance. To examine this possiblility, inspection of concurrent satellite sea surface temperature maps (Evans et al., 1984) confirms that the path of the Gulf Stream is approximately a curve of constant radius. Using the directional information contained in the acoustic doppler data, the center of rotation and the average radius of curvature is found by the 'center of momentum method' of Kennelly (1983). The likely size of a Gulf Stream 'cyclostrophic' term is estimated as about 0.02 the size of the Coriolis term in the momentum balance. Geostrophy still seems to be a good assumption even in this region of curvature; the correction from the addition of a V^2/R term would be at the noise level of our results.

We assume that any flow across the coastal boundary of our triangular region is negligible. The Slope Water ends of both hydrographic sections extend close to the 200 m isobath at stations 47 and 71 (fig. 1). Noting that Beardsley and Boicourt (1981) estimate the transport over the shelf to be 0.2 Sv, any transport across the shelf break should be insignificant relative to the huge fluxes across the south and north sections. To conserve mass within the area, the net mass fluxes across the two sections must be in balance.

(3.1) Direct Use of Acoustic Velocities

The average acoustic velocity between each station pair at the 100 db level can be used to reference the geostrophic calculations throughout the water column. After determining absolute velocities everywhere, the mass transports across the south and north sections are calculated. The total transports across each section are found to be out of balance by 50 Sv; since small errors in velocity cause huge errors in transport, this is not too surprising. As discussed previously, we suspect the acoustic velocities may contain a small systematic offset error consistently to one side of the ship. Since the ship traverses the two sections in opposite directions, the offset error would tend to increase the velocities along one section and decrease them along the other. By applying an offset error of 1.5 cm/s which decreases transport across the south section but increases it to the north, the net transports are balanced: 170 Sv across each. This systematic error is certainly within the bounds to be expected, and the total mass flux balance between the two sections is maintained. In the EN86 case,

Joyce et al. (1986) found this systematic velocity error to be 1.9 cm/s; the direct use of the acoustic velocities yielded a transport of 82 Sv across the EN86 south and north sections.

The resulting absolute velocity sections are shown in figure 5. We have achieved our goal of a complete synoptic view of the flow field across the south and north sections. We have removed a systematic error from the data, but an estimated random component of ±3 cm/s is still associated with the set of velocities between each station pair due to navigational uncertainties. This level of error in the velocity field unfortunately means we have little confidence in quoting transport calculations; ±3 cm/s in the velocity across the south section implies as much as ±39 Sv in transport uncertainty. The total net transport of 170 Sv does in fact seem high even for an instantaneous value. To examine aspects of the transport in different parts of the water column, the sections are divided into 13 layers defined by surfaces of constant potential density. Following Joyce et al. (1986), these layers are picked in an attempt to resolve the major water mass features; Table 1 lists the chosen isopycnals, average depths, and the mass transports across each section under 'direct acoustic'.

Assuming for the moment that the flow is entirely along these density layers, the transport within each layer should be in approximate balance between the south and north just as the total transport is. Figure 6 illustrates that the imbalances within each layer are in fact relatively large, particularly in some of the deep layers. Although a small amount of cross-isopycnal flow is expected, the vertical transports

required to yield a consistent picture are too large to be physically acceptable. To resolve this problem and to improve the accuracy of our velocity estimates, we get more information out of this data set through the use of inverse techniques.

TABLE 1

List of isopycnals and summary of mass transports within each layer, in units of 10^9 kg/s $\simeq 10^6$ m^3/s, positive north and east:

layer number	σ_θ	ave. depth of surface (km)	direct acoustic south	direct acoustic north	combined rank 33 south	combined rank 33 north	combined rank 36 south	combined rank 36 north
		surface						
1			5.2	4.8	5.2	4.7	5.1	4.7
	24.000	.020						
2			4.4	5.7	4.3	5.6	4.2	5.6
	25.000	.051						
3			31.1	28.8	29.2	28.9	29.5	28.4
	26.500	.291						
4			31.4	29.0	29.9	28.8	29.9	28.4
	27.000	.541						
5			13.2	12.7	12.6	12.0	12.4	12.1
	27.300	.684						
6			6.8	8.2	6.6	7.7	6.3	7.7
	27.500	.784						
7			8.9	10.1	8.4	8.3	8.0	9.1
	27.700	1.022						
8			9.1	11.6	8.7	8.9	7.9	9.9
	27.760	1.384						
9			10.8	14.8	9.5	11.5	8.9	12.3
	27.800	1.827						
10			16.0	16.7	13.7	12.8	13.1	13.3
	27.850	2.452						
11			11.5	8.6	9.1	6.2	9.3	6.2
	27.880	2.879						
12			3.8	7.1	4.9	6.1	5.0	5.1
	27.898	3.219						
13			17.5	11.5	11.1	11.7	12.6	9.6
		bottom						
Section totals:			170.0	170.0	153.0	153.0	152.0	152.0

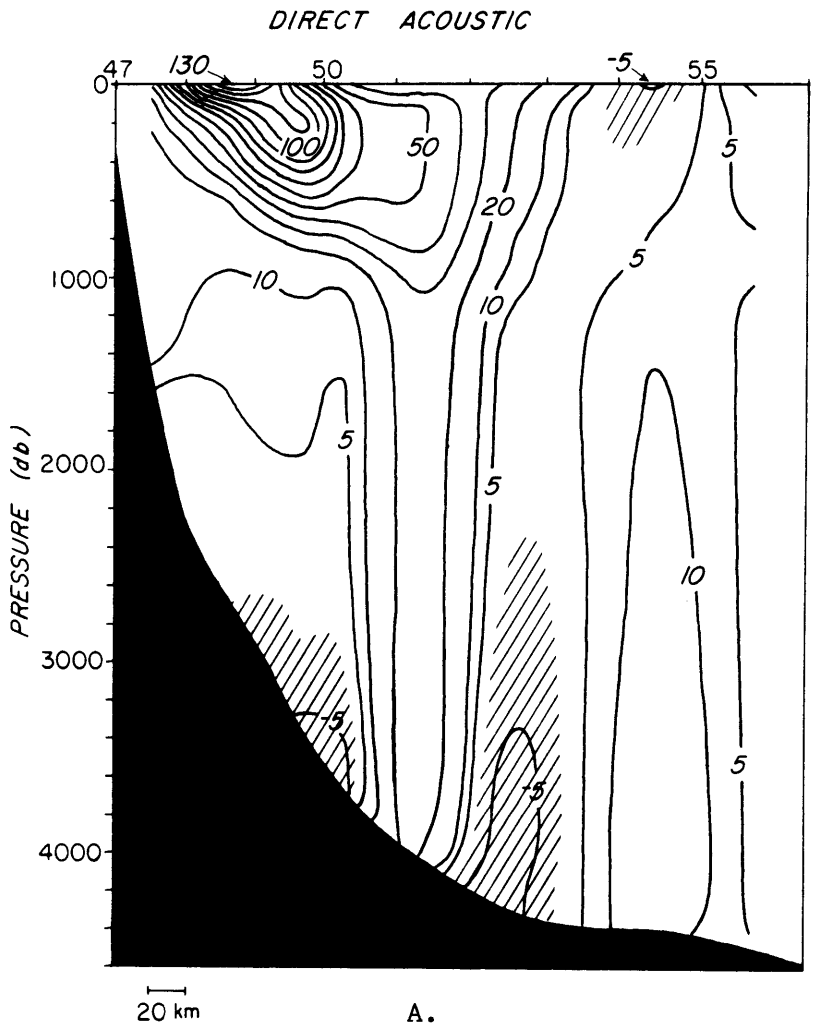

Fig. 5. Direct acoustically determined velocities (cm/s) normal to the south (a.) and north (b.) sections. A bias error of 1.5 cm/s has been removed from the velocity fields.

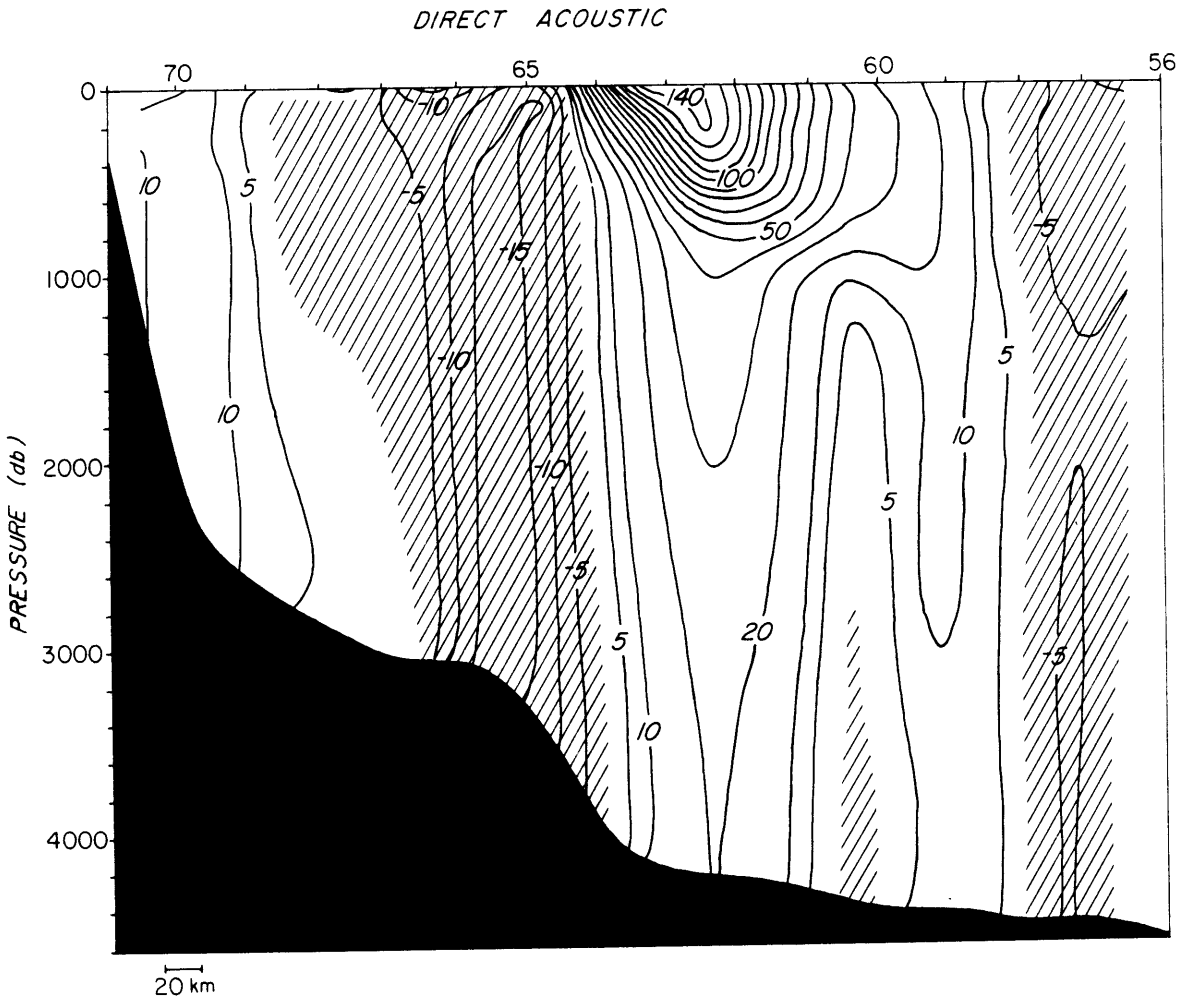
DIRECT ACOUSTIC
70
65
60
56
0
1000
2000
3000
4000
PRESSURE (db)
20 km
1
10
5
10
-10
-5
-15
-10
-10
-5
5
10
140
100
50
5
10
5
20
-5
5
10
-5

B.

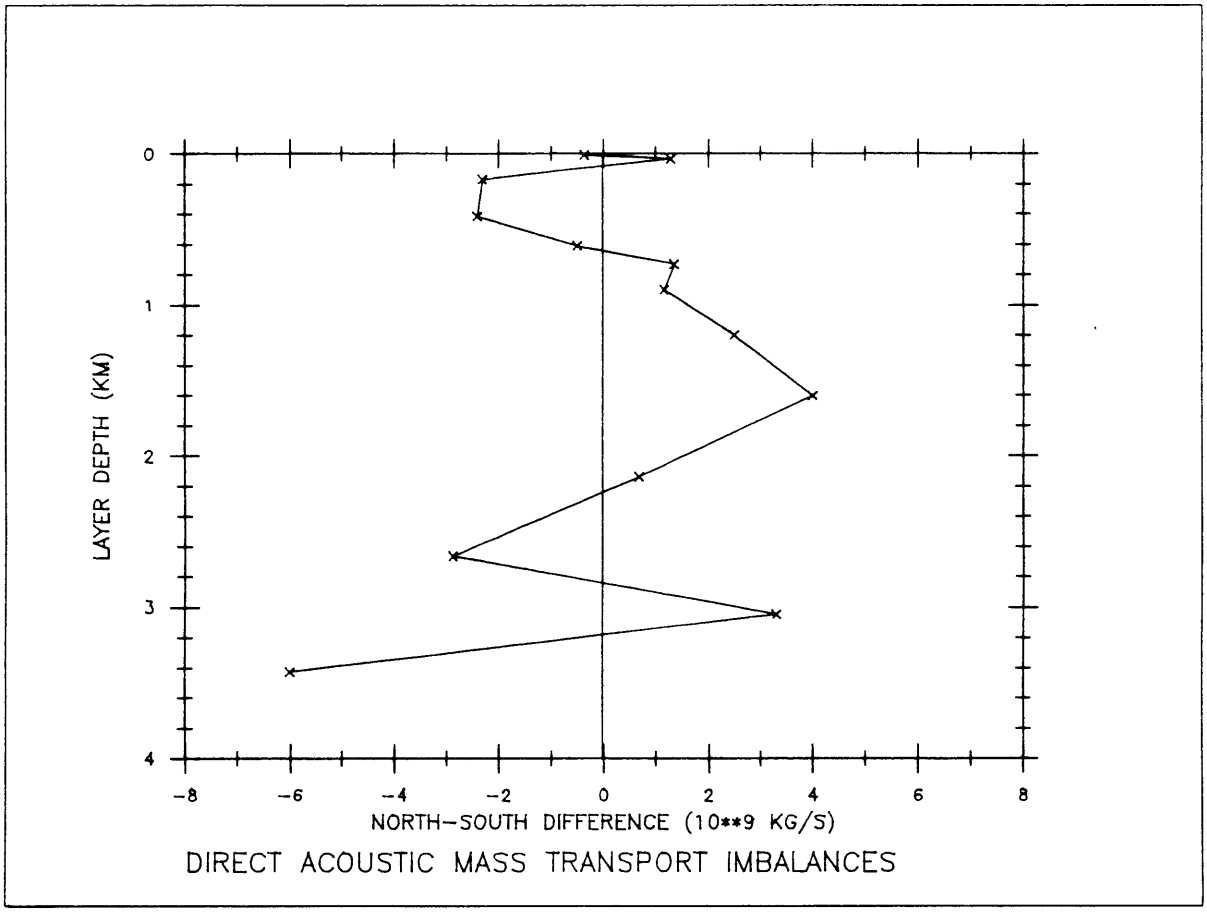

Fig. 6. Mass transport imbalances within each density layer using the direct acoustic velocities (10^9 kg/s $\simeq$ 10^6 m^3/s).

(3.2) Combined Inversion Technique

The inversion technique using the combined acoustic doppler and property data follows the same form as the procedures thoroughly developed by Wunsch (1978), Wunsch and Grant (1982), and Wunsch, Hu, and Grant (1983). The estimation method is based upon purely classical assumptions regarding the ocean circulation; these simple principles are applied in a formal and consistent manner. Conventional least-squares techniques are then brought to bear upon the problem to yield as much useful information as possible. Lawson and Hanson (1974) is a good reference for understanding the theory behind the solution of least-squares problems in general. The specific methods used here also closely follow those used by Joyce et al. (1986), who applied them to the similar EN86 data set.

The best estimate of the absolute flow field across the EN88 sections is required to satisfy the following set of constraints, all to within estimated errors:

(a) The horizontal velocity estimates are consistent with the direct acoustically measured ones.

(b) Total mass and total salt are conserved within our area.

(c) Mass and salt are conserved within each density layer.

(d) Oxygen is conserved within each layer, except for the top two shallow layers.

To begin the problem, the ocean is divided into density layers as listed in Table 1. To define the absolute flow field, we must solve for two sets of unknowns: the set of horizontal reference velocities, one for each station pair, and the set of cross-isopycnal velocities at each density surface, associated with between-layer transports. A discussion of the concept of a cross-isopycnal flow and its significance may be found in Wunsch et al. (1983). The horizontal reference velocities (at 100 db) are denoted as b_j, j=1,24 station pairs, and w_i^* is defined as the 'vertical' velocity across the isopycnal i between layers i and i+1, where i=1,12 isopycnals in the present case.

The constraint (a) that the acoustic velocities remain consistent with our results is expressed as

$$b_j = \alpha_j \pm \varepsilon_j, \quad j=1,24 \qquad (1)$$

where b_j is the true reference velocity for each station pair at the 100 db level, α_j is the acoustically derived velocity, and ε_j represents the error in the acoustics. As discussed previously, the errors ε_j are expected to contain a random component of ±3 cm/s and a systematic bias of about 1.5 cm/s.

The property conservation requirements (b)-(d) all take the form of linear equations balancing the inflow and outflow from any given layer. Let a generalized 'area' a_{ij} be defined as the area in the vertical plane within station pair j occupied by the property in layer i and multiplied by its concentration there. An analagous a_i' is the 'area' of the isopycnal surface i. Then a generalized form for the

conservation of a given property within a given layer i may be written:

$$\sum_{j=1}^{24} a_{ij}\phi_j(b_j + v_{ij}) + a'_i w_i^* - a'_{i-1} w_{i-1}^* \simeq 0 \qquad (2)$$

where: $\phi_j = \pm 1$ represents the sign of the unit normal to the volume, and v_{ij} is the thermal wind component of the velocity such that $(b_j + v_{ij})$ represents the true geostrophic velocity.

Let our combined set of unknowns b_j, w_i^* be written as a column vector

$$\underline{q} = \begin{vmatrix} \underline{b} \\ \cdots \\ \underline{w}^* \end{vmatrix}$$

Now we can express the set of conservation requirements (2) as

$$\underline{A}\underline{q} + \underline{\Gamma} \simeq 0 \qquad (3)$$

where: $\underline{A}$ is a matrix made up of the elements a_{ij}, a_i' for each of the properties (mass, salt, O_2), and $\underline{\Gamma}$ represents the initial imbalances of the properties given only the thermal wind component v_{ij}. The approximation sign used in (3) represents explicitly that the conservation constraints are only maintained to within a certain level of error. To make an a priori estimate of the size of these errors, we consider a number of possible sources. Since the CTD/O_2 stations were occupied over a period of 4 days, there could be some temporal aliasing; this region is known for its time variability. Satellite data from the RSMAS remote sensing group (Evans et al., 1984) during the period confirms this, indicating a shift of the shoreward edge of the Gulf Stream by about 20 km to the east along the south section. In the top two density layers we do not require oxygen conservation at all due to the

surface mixing; mass and salt conservation might also be adversely affected here. Finally, various observational errors associated with the property data contribute to the uncertainty of equations (3). We end up making a rough estimate that in the deeper layers the mass transport should be maintained to ±0.3 Sv, while in the top two layers we only expect conservation to ±0.9 Sv. The total mass conservation of all layers combined is a better assumption and we estimate it is maintained to ±0.1 Sv. For the salt and oxygen transports, we predict levels of error non-dimensionally equivalent to those for the mass transports.

The set of equations (3) defines the pure geostrophic inverse problem where only property data are observed. As Wunsch (1978) is quick to point out, however, the method allows for the addition of any other information about the ocean that might be available. In this case we have the set of 24 acoustic constraints (1) which can be combined with the set (3), forming the new problem

$$\underset{\sim}{A}'\underline{q} + \underline{\Gamma}' \simeq 0 \qquad (4) \qquad \text{where: } \underset{\sim}{A}' = \begin{vmatrix} \underset{\sim}{I}_{24} : \underset{\sim}{0} \\ \cdots : \cdots \\ \underset{\sim}{A} \end{vmatrix}, \quad \underline{\Gamma}' = \begin{vmatrix} \underline{\alpha} \\ \cdots \\ \underline{\Gamma} \end{vmatrix}$$

$\underset{\sim}{I}_{24}$ is the 24x24 identity matrix
$\underset{\sim}{0}$ is the 24x12 null matrix

For each of equations (4), a row weighting factor is introduced which is inversely proportional to the estimated error in that constraint; the set of equations becomes non-dimensional. This step requires the estimation of error levels a priori, as discussed above. A column weighting is also imposed upon the solution space of the system in the interest of numerical stability; weighting among the b_j corrects for the artificial tendency of the solution to favor larger magnitudes in

the deeper station pairs (Wunsch, 1978). The relative magnitudes expected for the b_j as opposed to the solution w_i^* are also reflected in the column weighting scheme. If the system is in fact overdetermined, the column weighting has no effect on the solution; it is only of significance for underdetermined problems. Lawson and Hanson (1974) fully discuss all of these points.

To solve the system of equations (4), the singular value decomposition (SVD) method is used (Wunsch, 1978); this technique is one which allows a complete analysis of the structure of a solution. The SVD solution takes the form

$$\underline{q} = \sum_{1=1}^{k} \underline{V}_1 \frac{[\ \underline{U}_1^T\ (-\underline{\Gamma})\ ]}{\lambda_1} \qquad (5)$$

where: $\underset{\sim}{A}\underset{\sim}{A}^T\underline{U}_1 = \lambda_1^2\underline{U}_1$, $\underset{\sim}{A}^T\underset{\sim}{A}\underline{V}_1 = \lambda_1^2\underline{V}_1$

and $\underset{\sim}{A}\underline{V}_1 = \lambda_1\underline{U}_1$, $\underset{\sim}{A}^T\underline{U}_1 = \lambda_1\underline{V}_1$

The rank k of the system represents the number of non-zero singular values λ; k also equals the degree of linear independence among the constraint equations. The value of k must be determined to know where to stop the summation of (5). If k is known, the SVD yields the solution that simultaneously minimizes the solution norm and the residual norm, respectively

$$||\underline{q}|| \quad , \quad ||\ \underset{\sim}{A}\underline{q} + \underline{\Gamma}\ ||$$

The system (4) consists of a total of M = 63 constraint equations in N = 36 unknowns. The degree of independence among the constraints is defined by the rank k; if k is actually equal to 36, the system is a fully determined one, a regression problem, whereas if $k < 36$ we have a rank deficient or inverse problem. A number of methods can be used to

estimate the rank of a problem (Lawson and Hanson, 1974). One of the methods used here is the Levenburg-Marquardt analysis illustrated in figure 7. The curve indicates the magnitude of the residuals left in the constraint equations vs. the solution magnitude, for the range of possible solutions. The optimal solution to a least squares problem is interpreted to be the one lying at the base of the steep decrease in residual (fig. 7); at this point the solution magnitude is increasing only slightly to yield a great reduction in residual. In our case this point occurs almost at the end of the curve, indicating a nearly fully determined problem. The rank 33 solution lies just at the base of the steepest part of the curve. The rank 36 choice, however, is only slightly beyond this point; a small increase in solution norm allows the rank 36 solution, which represents a fully determined system. While the evidence is strong that the rank of the system is somewhere between 33 and 36, it is difficult to decide exactly where; other methods of analysis yield a similar uncertainty. Fortunately, we will discover that the solution is actually relatively stable within this range, insensitive to the exact choice of rank. Both the rank 33 and 36 solutions are presented, representing the limits of our uncertainty.

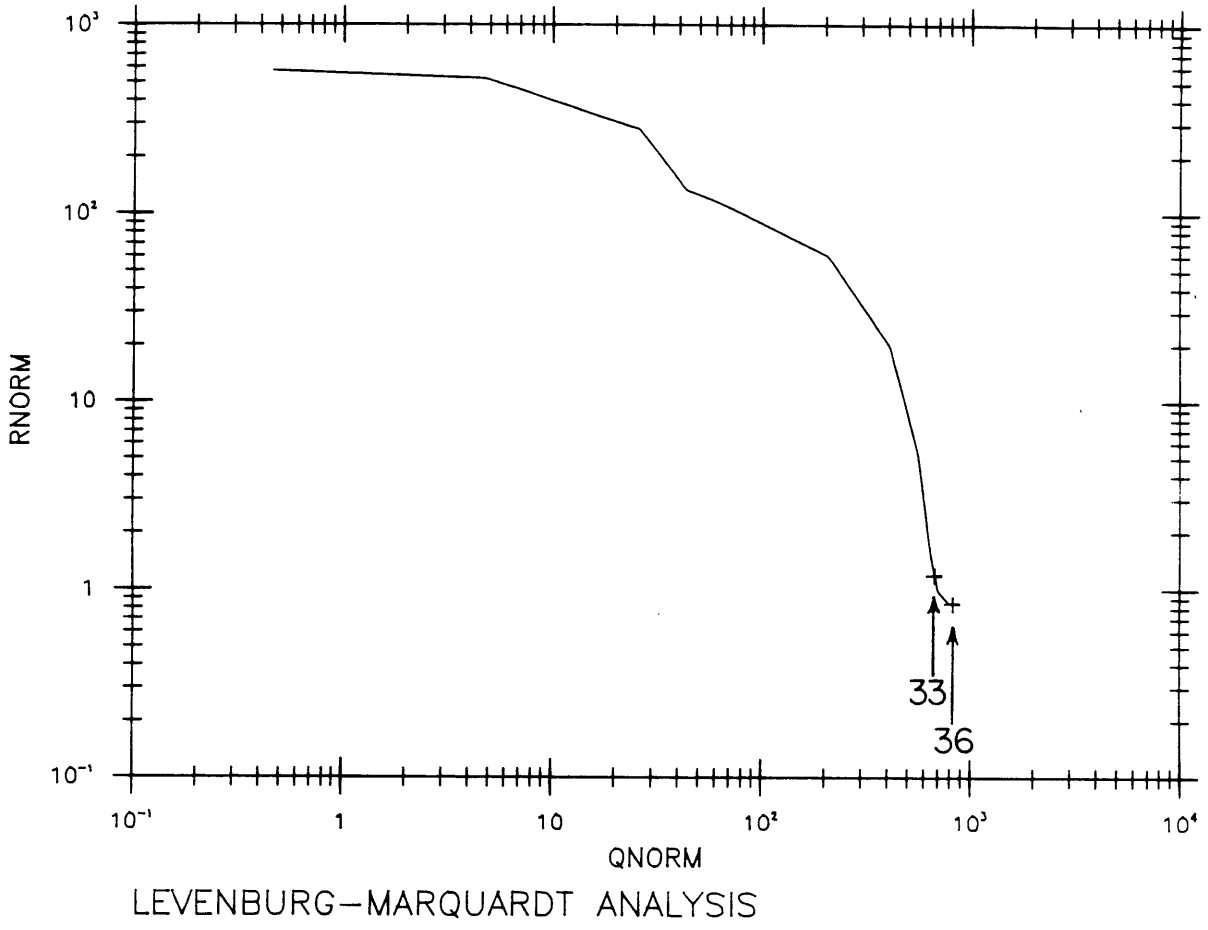

Fig. 7. Levenburg-Marquardt analysis showing the decrease in residual norm with increasing solution norm. The arrows mark the locations of our rank 33 and rank 36 solutions on this curve.

4. Results of the Combined Inversion

The calculated reference velocities $\underline{b}_j$ in conjunction with the thermal wind yield the absolute velocity sections of fig. 8 (rank 33) and fig. 9 (rank 36). Once again we have a complete picture of the synoptic flow field across the sections. The differences between these velocity fields and the direct acoustic ones of fig. 5 are qualitatively very slight. Referring to Table 1, however, we note some significant changes in the mass transports. The total transports for the combined inversions are decreased by about 20 Sv from the direct acoustic case, while the north vs. south fluxes for each layer reveal greatly reduced imbalances. Moreover, the imbalances that exist are a result of cross-isopycnal mass transfers that are explicitly solved for by the calculation; the w_i^* are shown in fig. 11.

The SVD technique also provides us with full information regarding the nature and accuracy of our solution. In equation (5) we introduced the column vectors $\underline{U}_1$ and $\underline{V}_1$ in our statement of the SVD solution. In the SVD these vectors make up matrices of dimensions M and N respectively, where M is the number of constraints and N is the number of unknowns (Wunsch, 1978). It can be shown that the diagonal elements of $\underline{UU}^T$ and $\underline{VV}^T$ have a straightforward interpretation; the rank k of the solution will be such that $k = \text{trace}\underline{UU}^T = \text{trace}\underline{VV}^T$. Each diagonal element of $\underline{UU}^T$ corresponds to one of the constraints, and the value of this element is a measure of the contribution of this constraint to the total solution. Similarly, the values of the diagonal elements of $\underline{VV}^T$ give a measure of how well resolved each of our unknowns is; if $k < N$,

the rank k will be split up amongst the N elements according to our confidence in each of the N solution elements.

By inspection of the diagonal values of $\underline{U}\underline{U}^T$, we summarize in Table 2 the contribution of each set of constraints to the solution. The direct acoustic case is included simply as a suggestion that we can think of this as an inverse problem using only the acoustic velocities as constraints. In the rank 33 and 36 solutions, we note that the mass and salt equations contribute roughly equal amounts; this is not surprising since the mass and salt equations are actually highly correlated. Oxygen contributes less since fewer equations were written for it. The dominant contributions come from the acoustic equations; they are still providing most of the information for our solution. We note how much less information we would have available without the acoustics; a pure hydrographic inversion is typically a largely underdetermined problem. The direct acoustic column, on the other hand, reminds us of how poorly we do using only the acoustic data. Each set of constraints contributes significantly to our result.

TABLE 2

Contribution of each category of constraint to the total solution:

constraints	direct	acoustic	rank 33	rank 36
Mass layers 1-13 & total	-		5.05	5.39
Salt layers 1-13 & total	-		4.93	5.10
Oxygen layers 3-13	-		2.94	3.39
Total property conservation	-		12.92	13.88
Acoustic velocities		24	20.08	22.12
Total rank		24	33	36

Figure 10 presents the values of the rank 33 and 36 solution b_j's relative to the direct acoustic values; these are the residuals left in the set of acoustic constraints. In the rank 33 case the acoustic values are maintained with a bias error of -1.7 cm/s across the south section, 0.4 cm/s across the north, and a random component of ±3.0 cm/s overall. For rank 36 the biases are -2.3 cm/s and 0.7 cm/s and the random error is ±1.9 cm/s. These biases are of the correct sign and magnitude to be explained by the transducer angle error. The random components of the residuals are consistent with our estimate of navigational uncertainty; in the rank 36 case the ±1.9 cm/s is even better than we predicted.

The representative error bars shown on fig. 10 indicate our formal confidence in any particular reference velocity; this is typically ±1-2 cm/s. In the rank 33 or underdetermined case, the error bars have two contributors; the failure to be fully resolved and the observational noise. Inspection of the $\underline{VV}^T$ diagonal elements reveals that at rank 33, nearly all of the b_j's have been determined to 0.999 or better. The only exception to this is the middle of the three error bars shown for the south section (fig. 9a); this velocity is only resolved to 0.946, which implies ±8.6 cm/s has been left undetermined. The remaining error for this b_j and the dominant error associated with every other b_j is due to observational noise. The solution technique determines the variance due to inaccuracies in the data explicitly (explained by Wunsch, 1978). For rank 33 this is typically ±1.7 cm/s and for rank 36 it is ±1.4 cm/s. Since rank 36 is the fully determined case, there is

no error from lack of resolution; all unknowns are formally resolved. The difference between the rank 33 and rank 36 solutions in fig. 10 can be taken as an additional uncertainty due to our inability to choose the rank exactly.

The reference velocity that deviates the most from the acoustic value is between stations 51-52 (5^{th} from the left on fig. 9a). Inspection of the raw doppler data reveals that for stations 51-52 the data return within our 10 minute averaging blocks was at its lowest; at the 60 m depth only 46% of the emitted pulses were being received, vs. an overall section average of 68% return. The amount of scattering material present was at a minimum, and apparently the accuracy of the doppler estimate begins to be affected at this level. The difficulty that the combined inversion technique had in resolving this particular velocity has taught us something about the quality of the acoustic data.

The cross-isopycnal mass transfers w_i^* are also presented with some representative error bars (fig. 11). In the rank 33 case the solutions are dominated by the errors, making most of the values indistinguishable from zero; the w_i^* tend to be less well resolved than the horizontal velocity components. In the fully determined case we see a broad structure to the solution with generally positive values in the deep water and some downward transfer among the top few layers.

To summarize the vertical distribution of the horizontal transports, the flux densities per unit depth are given for mass, salt, and oxygen (fig. 12a-c). These are integrated flux densities across the whole south and north sections for each layer; the mass flux densities

multiplied by the thickness of each layer will yield the transports found in Table 1. The salt and oxygen flux densities have very similar structure to the mass case, illustrating the redundancy inherent in the flux budgeting constraints. Although much of the structure of the solution is lost in the section average, we note the increase in the transport density among the upper layers from south to north, corresponding to the thinning of these density layers. Another interesting feature is the noticeable minimum of layer 12 in the south sections, representing the effects of southwestward moving water within this layer.

Useful information about the structure of our inverse solution can sometimes be gained by study of the residuals left in the property constraints. The residuals left in the mass, salt, and oxygen conservation equations for each layer are shown in fig. 13. We see that the constraints have been maintained well below our a priori requirements of ± 0.3 Sv or the equivalent salt/O_2 levels, another check on the consistency of our solution. Beyond this, the residuals represent those aspects of the data set which have not been explained by our solution; if we feel that we have extracted all of the useful information out of our data, the residuals should appear to be random noise. The mass residuals (fig. 13a) for either the rank 33 or 36 cases do not appear random; some sort of structure with depth is apparent. Since rank 36 is the fully determined case, any remaining structure in the residuals might indicate missing physics from the model. While the magnitude of the residuals is slightly less at rank 36, the structure is not diminished; the modifications to our model that might be indicated are some sort of mass storage

terms with depth. Considering we are at the level of ±0.1 Sv, however, it does not seem worthwhile to attempt a more sophisticated model.

The residuals for salt and oxygen (fig. 13b-c) also exhibit some organized structure, but they are different from the mass residuals. These differences might reflect the fact that different rates of cross-isopycnal flux occur for each of the properties. While the residuals for oxygen are somewhat large, they correspond well with some ideas regarding the non-conservation of oxygen: production of O_2 near the surface, consumption in the deeper water, and the minimum of layers 5 and 6 agrees with the oxygen concentration minimum at about this level (see figs. 3c or 4c).

We have presented solutions throughout for both the rank 33 and 36 cases, and the inspection of our results confirms the difficulty in choosing the exact rank of the problem. The two cases are remarkably similar, and neither one seems clearly more appropriate. Joyce et al. (1986) in the EN86 case also found an uncertainty associated with the choice of rank; they present both the rank 25 and rank 30 solutions in their results. The difference between the rank 33 and 36 cases represents our uncertainty; although small, this is the largest formal uncertainty associated with the calculation.

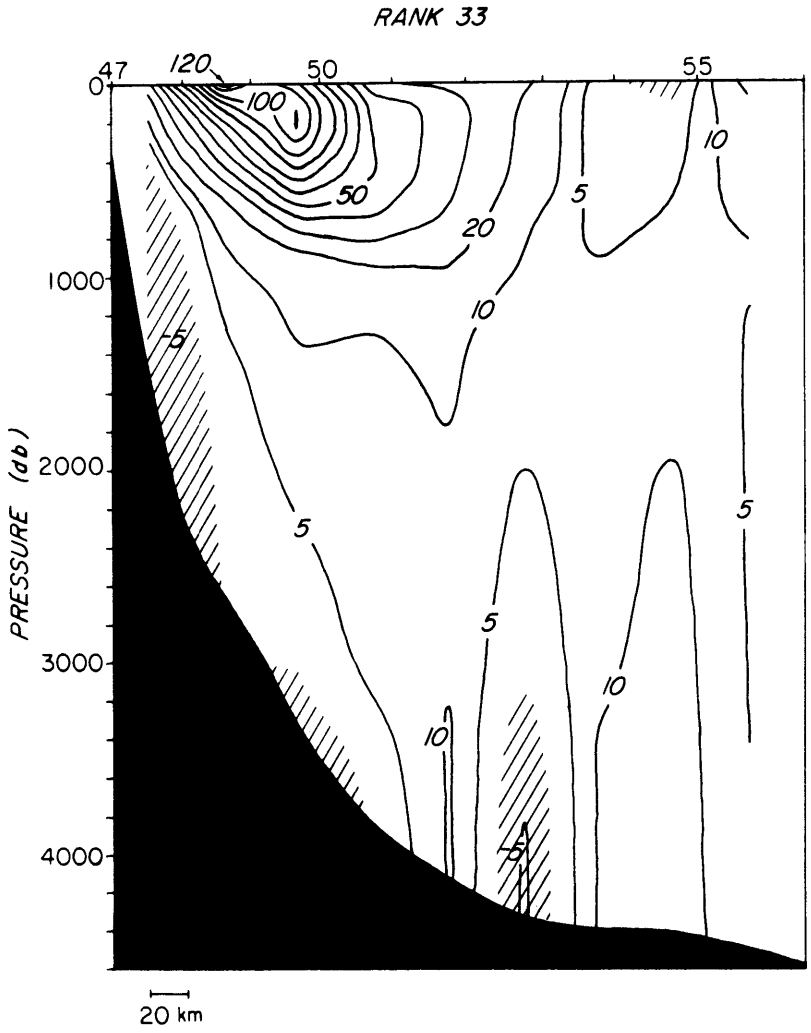

A.

Fig. 8. Rank 33 combined inversion velocity (cm/s), normal to the south (a) and north (b) sections.

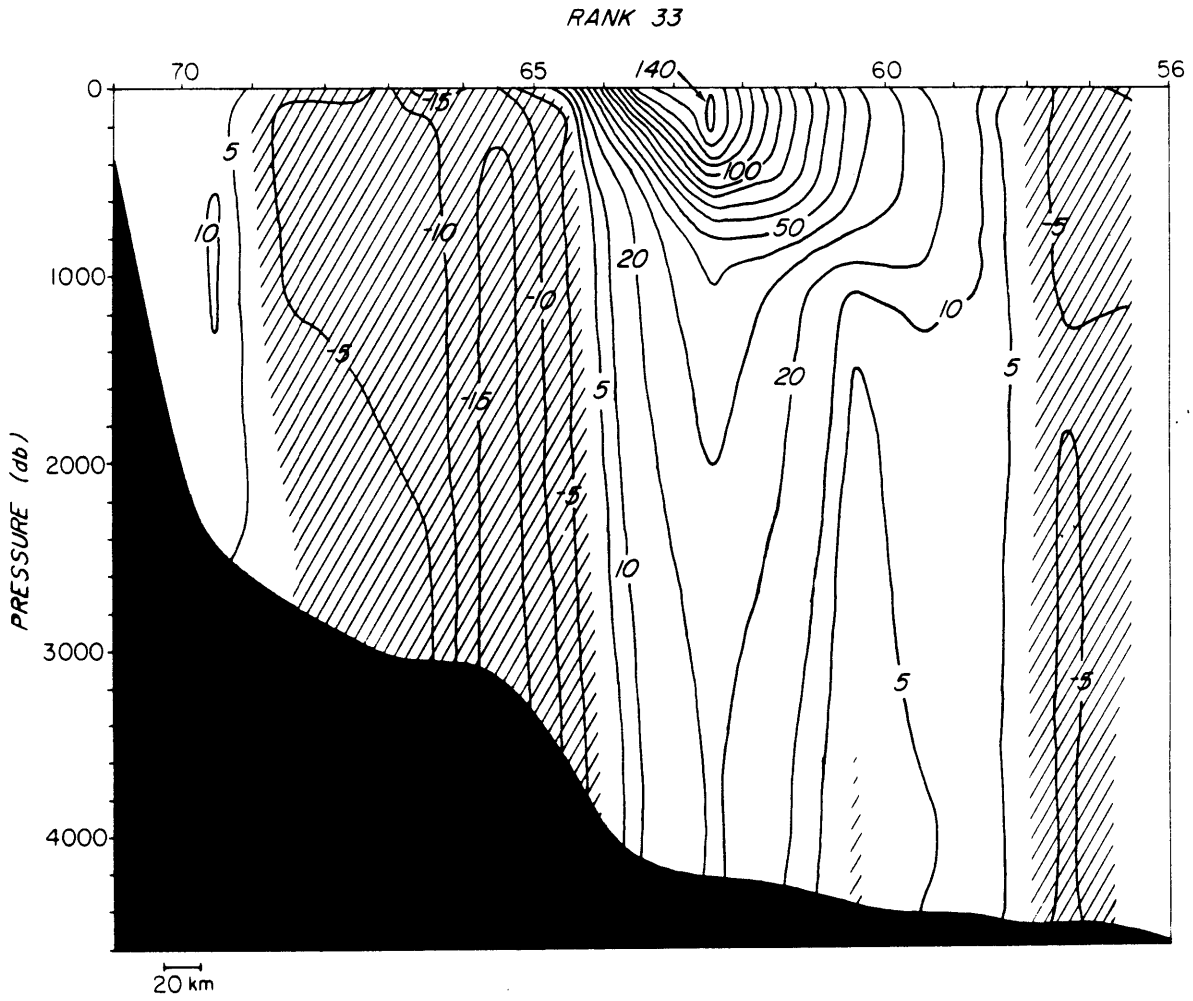
RANK 33
70
65
60
56
0
1000
2000
3000
4000
PRESSURE (db)
140
100
50
20
10
5
-5
-10
-15
20 km

B.

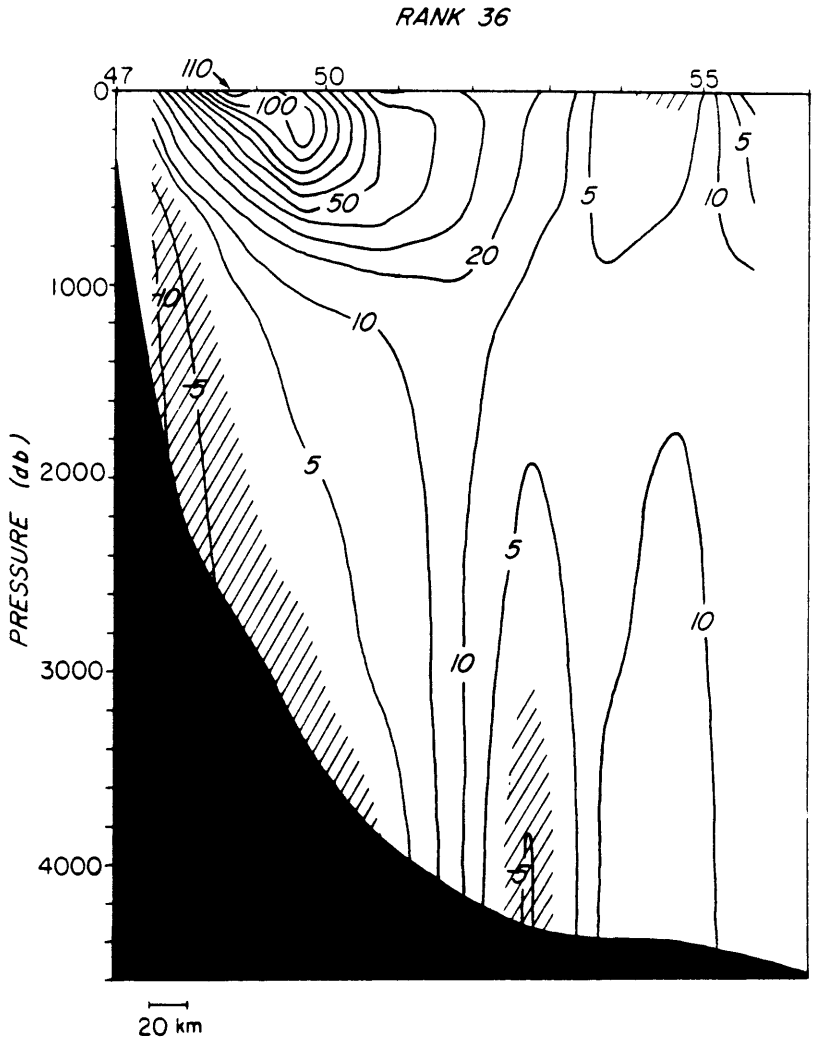

A.

Fig. 9. Rank 36 combined inversion velocity (cm/s), normal to the south (a) and north (b) sections.

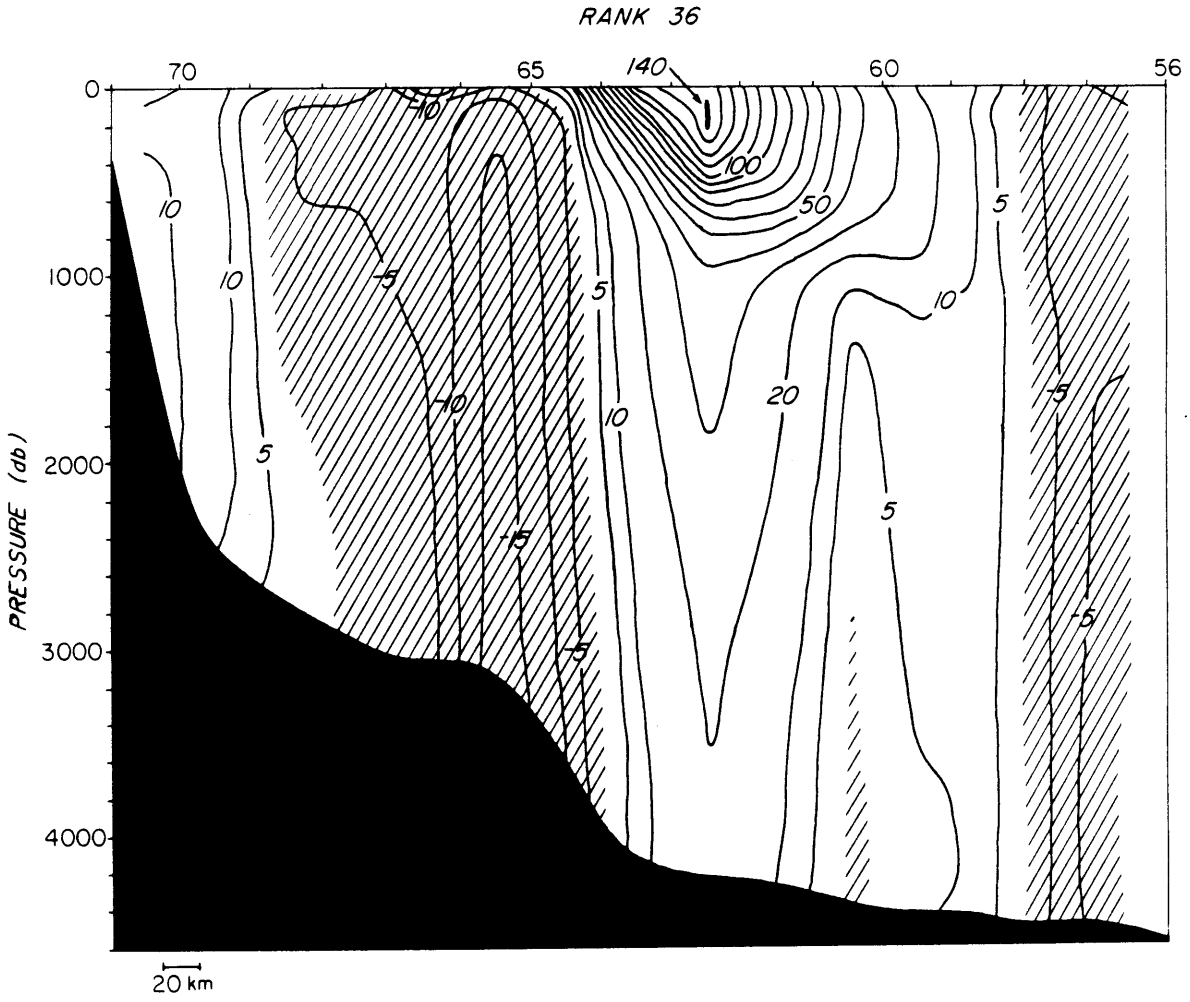

B.

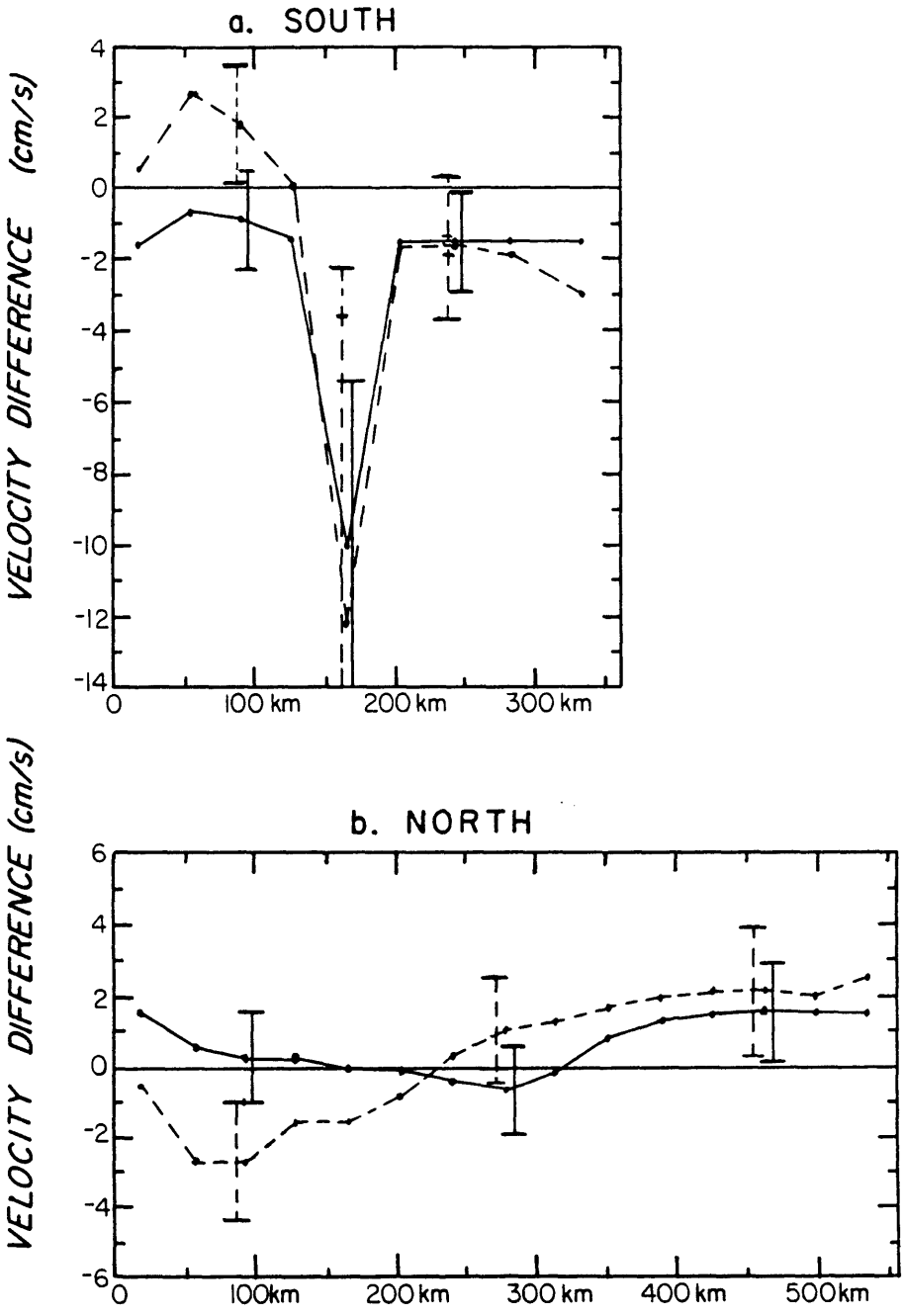

Fig. 10a-b. Differences between the rank 36 (solid) and rank 33 (dashed) solutions from the direct acoustic values. Two sets of error bars are shown for the rank 33 case; inner set is due to failure to resolve, while outer set includes additional error due to observational noise. Error bars for the rank 36 solution are wholly due to noise, since this is the fully determined case.

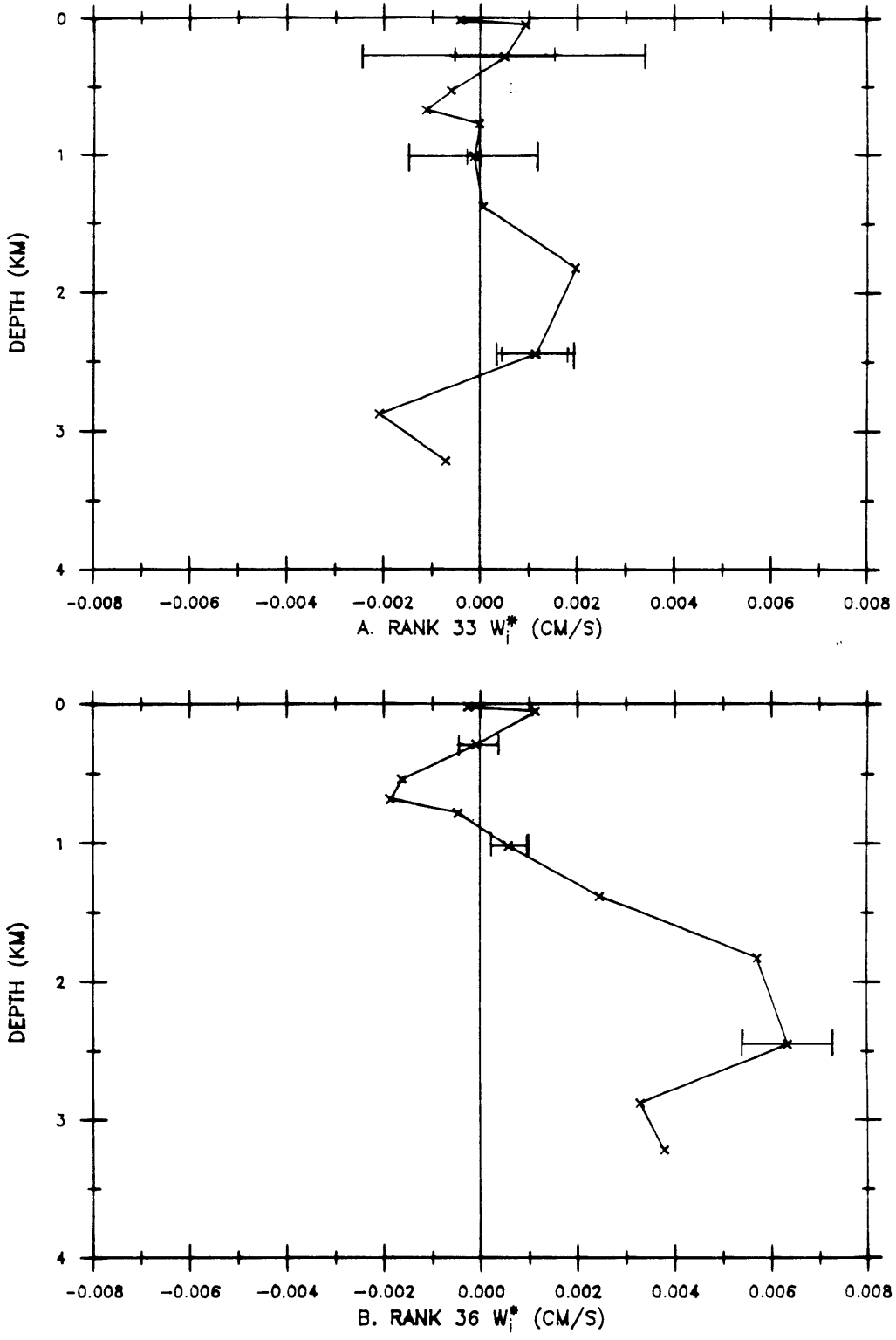

Fig. 11. Vertical mass transfers across isopycnal surfaces for the rank 33 (a) and rank 36 (b) case. Error bars follow convention of fig. 10.

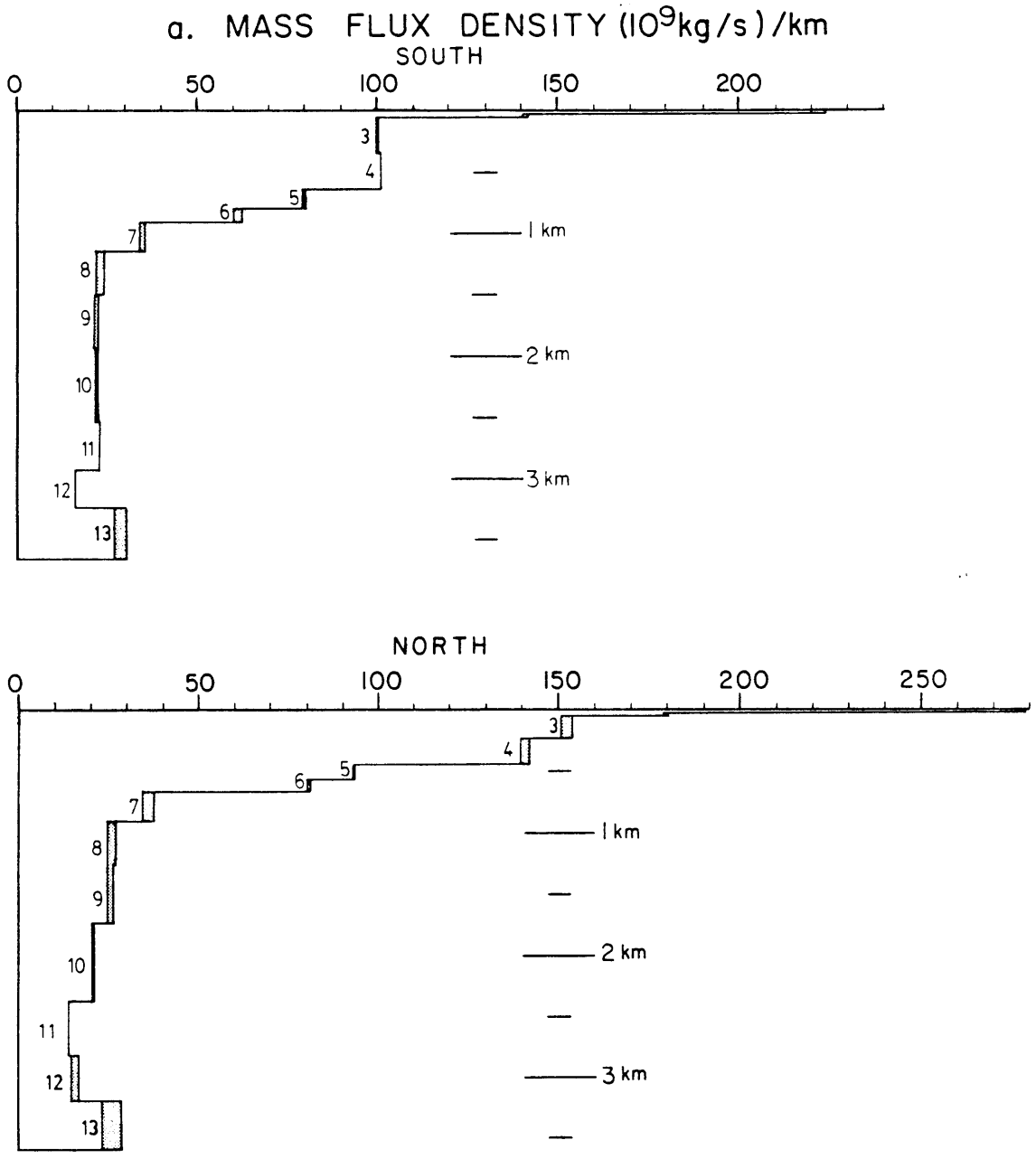

Fig. 12. Layer flux densities per unit depth for mass (a), salt (b), and oxygen (c). Shading represents difference between ranks 33 and 36. Properties are scaled with equivalent units.

b. SALT FLUX DENSITY 10^6 kg/s/km

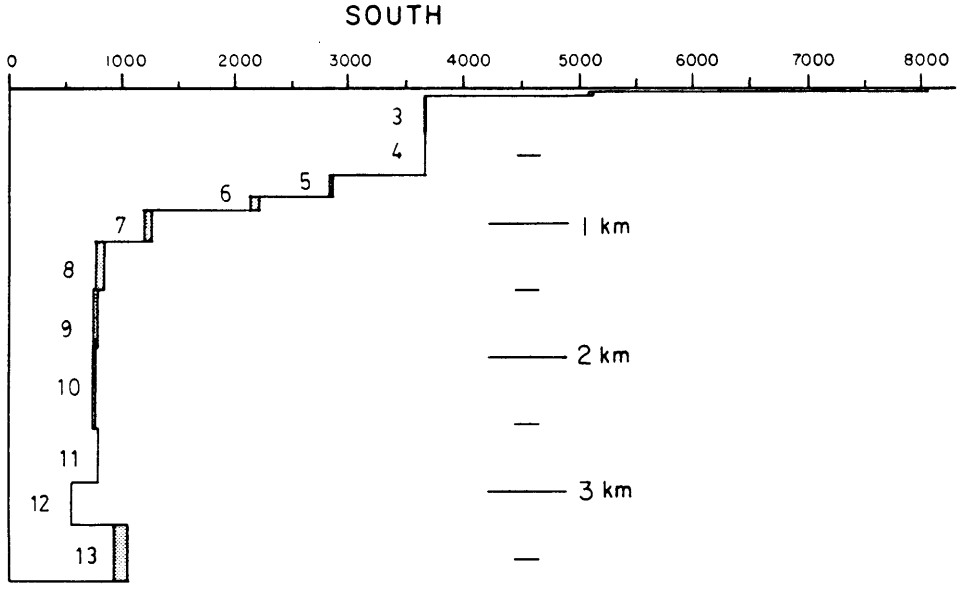

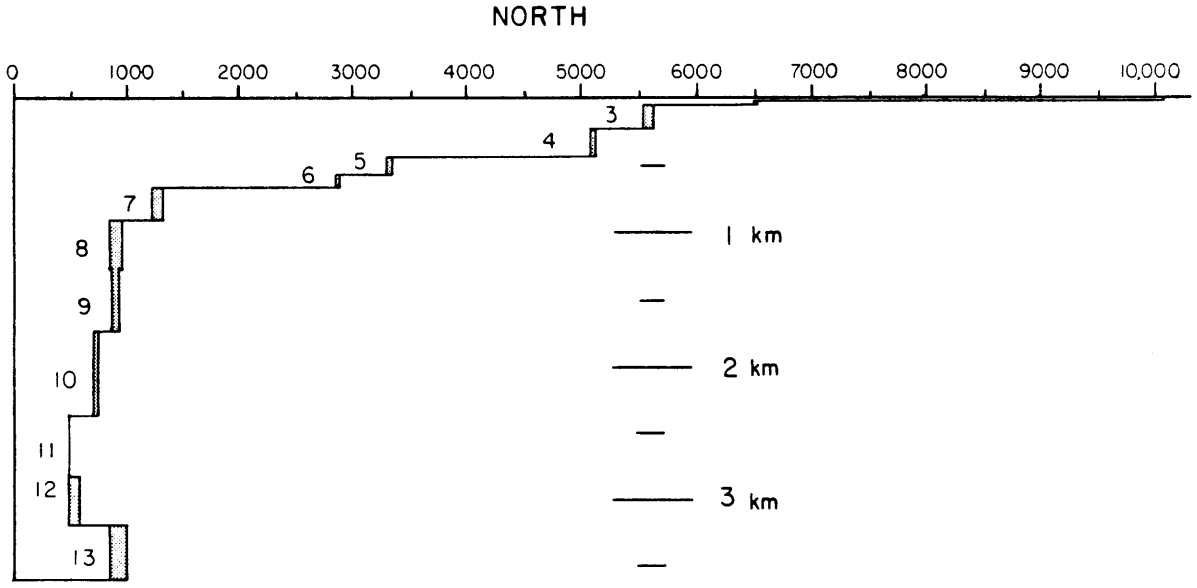

c. OXYGEN FLUX DENSITY (ml/l) x 10^9kg/s/km

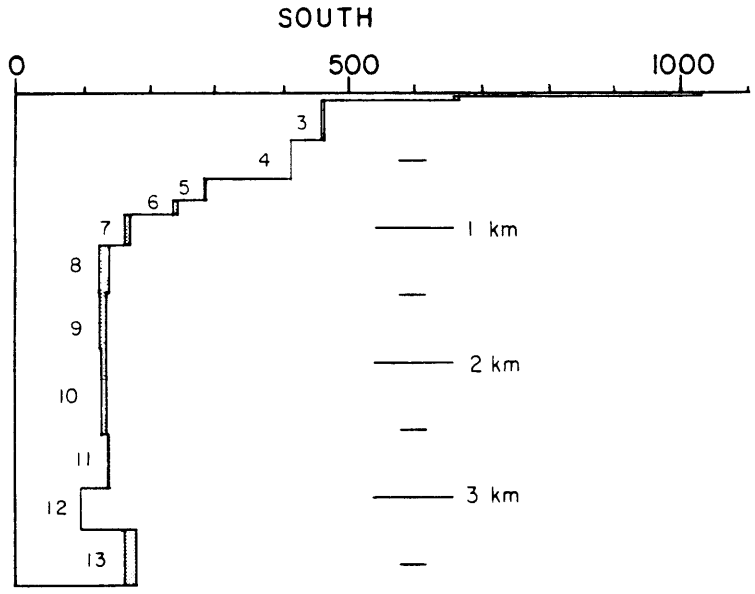

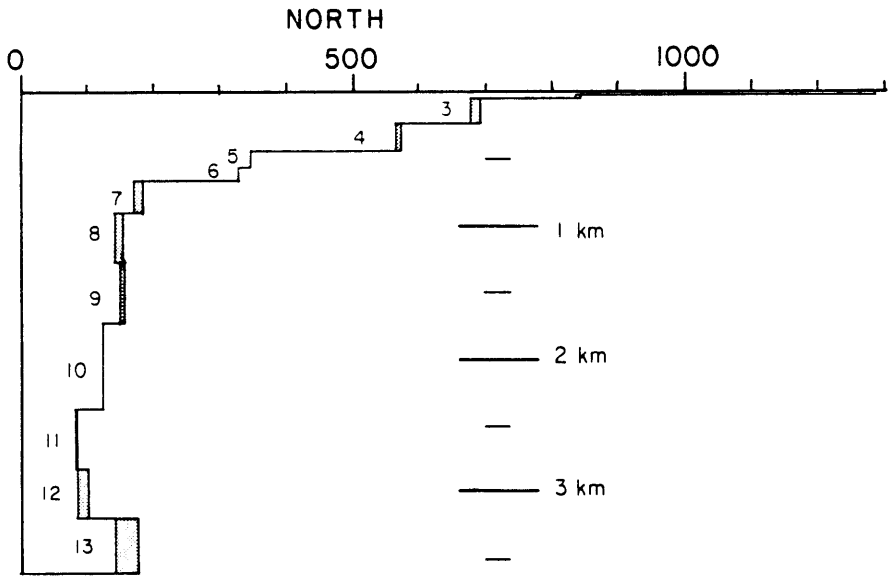

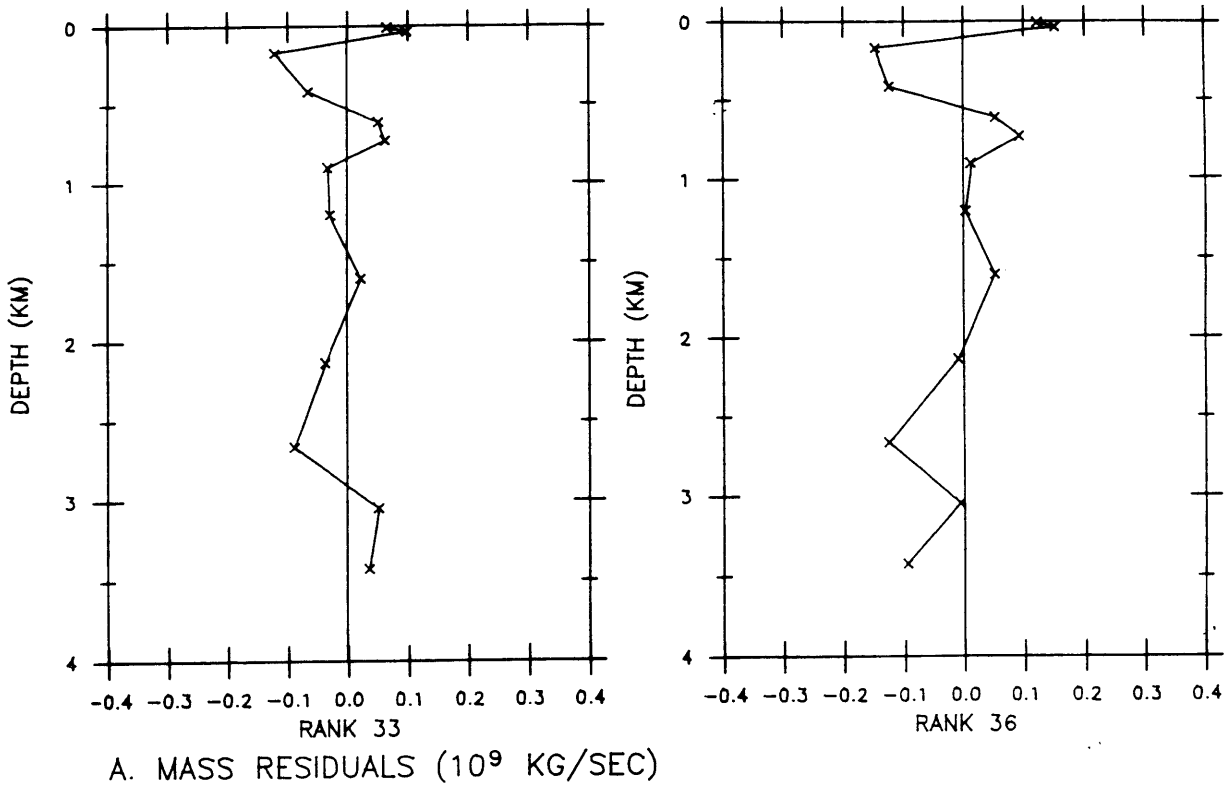

A. MASS RESIDUALS (10^9 KG/SEC)

Fig. 13a-c. Residuals left in the conservation constraints for mass, salt, and oxygen. Properties are scaled using equivalent units. Compare (a) to fig. 6.

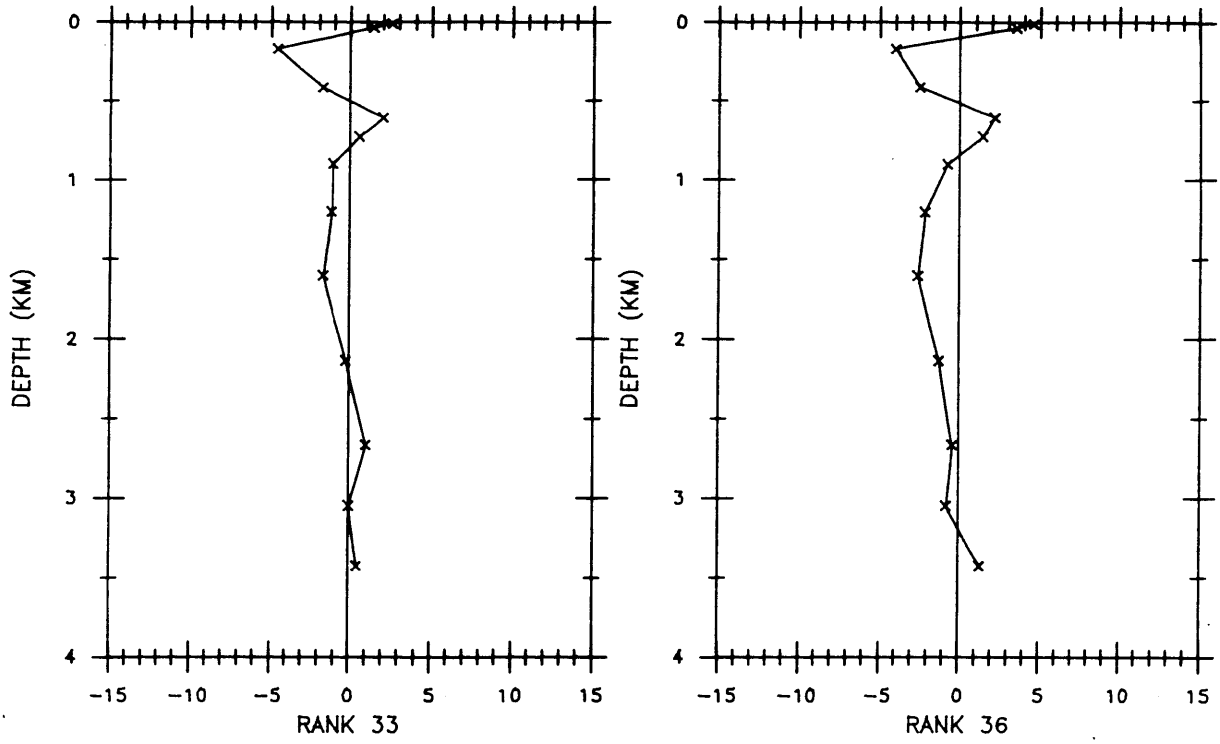

B. SALT RESIDUALS (‰ X 10^9 KG/S)

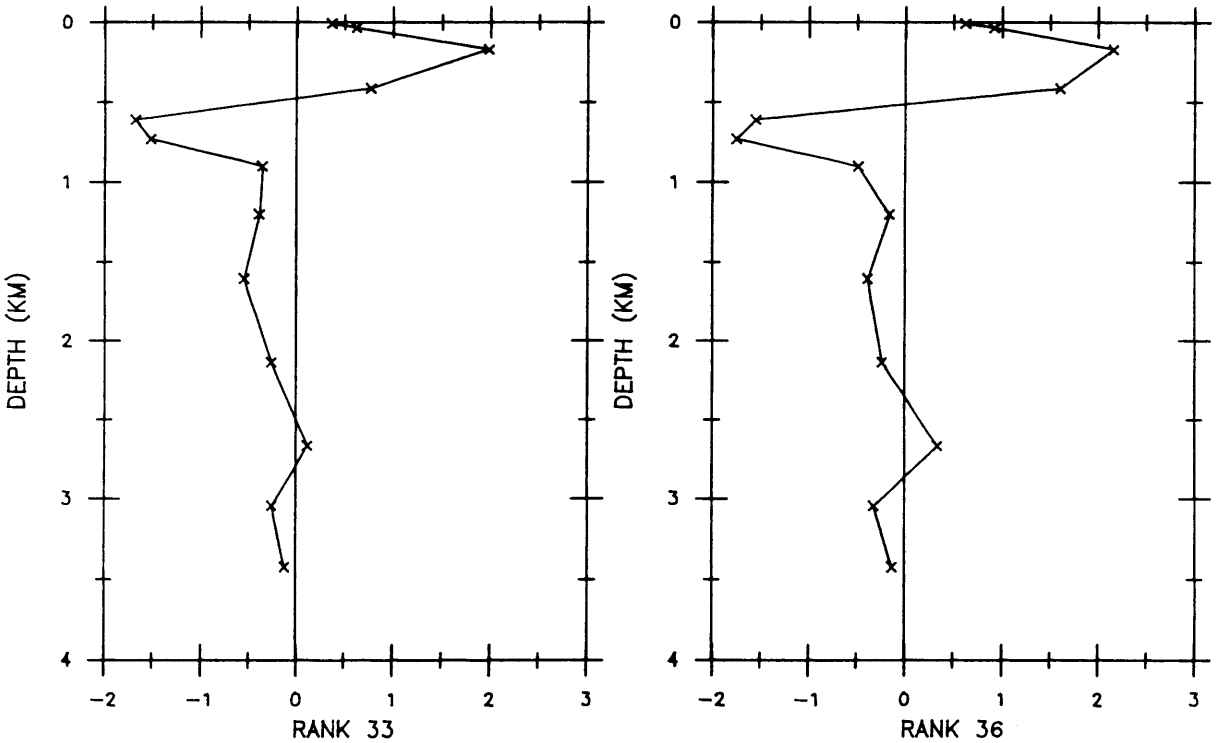

C. OXYGEN RESIDUALS (ML/L X 10^9 KG/S)

5. Discussion: the Synoptic Flow Field

Through the combined inversion we have achieved our best possible estimate of the synoptic flow field off of Cape Hatteras on 20-25 August 1982. We emphasize that this is a nearly instantaneous description of the flow field and does not represent an average condition; the region is well known for its time variability. Yet large-scale features of our solution can be usefully compared with ideas about the time-average condition.

Our velocity sections (figs. 8,9) reveal a Gulf Stream core moving at speeds as high as 110 cm/s across the south and 130 cm/s across the north. The Gulf Stream flow extends to the bottom on both sections, and to the north we see an especially strong eastward flow at the bottom. In the deep waters of the south section, two components of southwestward flow of high oxygen water are evident, identifying the Deep Western Boundary Current (DWBC). The stronger of these is just east of the Gulf Stream axis between stations 52 and 54, while further up the Slope is the other component, better defined at rank 36 than 33. To the north, the deep westward flow appears in a number of places but is concentrated between stations 65 and 69; here it is part of a nearly barotropic southwest flow in the Slope Water region. This feature is consistent with the mean flow across 70°W presented by Hogg (1983), exhibiting both a surface-intensified westward velocity and a slight bottom intensification. South of the deep Gulf Stream between stations 59-60 is a secondary eastward flow extending to the bottom; this happens to correlate well with one of the deep long-term current meter records used by Hogg (1983).

The combined inverse solution also offers us a picture of the vertical water movements (fig. 11). Although the uncertainties are relatively large and mass transfer w_i^* is not strictly a vertical velocity, fig. 11b displays some similarity to conventional beliefs; the consistent upwelling in the deep water is particularly encouraging. The magnitudes of the w_i^*'s do seem large for typical vertical velocities, but this is not a typical region, and these could be consistent with the large velocity shears associated with a western boundary current. Joyce et al. (1986) also present vertical mass transfers for the region; their results are in rough agreement but also include downward velocities among the bottom few layers rather than the broad upwelling of fig. 11b. Since our range of uncertainty is between figs. 11a and 11b, it is not possible to make a definitive statement regarding the vertical mass transfer.

In the thorough analysis made by Hall (1985) of the data set from the GUSTO mooring at 68°W, vertical velocities are derived theoretically from the measured horizontal currents and temperatures. Although these values are found through completely different methods, they compare well with our results. Hall (1985) calculates average vertical velocities of -4.4×10^{-3} cm/s at 575 db, 3.5×10^{-3} cm/s at both 875 db and 1175 db, and -6.7×10^{-3} cm/s at 2000 db. Our results agree with the downwelling in shallow water as well as the upwelling at mid-depths, while the negative velocity at 2000 db is more like the result of Joyce et al. (1986). Also reassuring are the similar large magnitudes for the vertical velocities found by Hall in this region.

The total horizontal mass transport across both of our sections is 152 ± 1 Sv (Table 1.). The narrow range of uncertainty between the rank 33 and 36 solutions is another indication that the total mass conservation assumption is an excellent one. We present fig. 14 as a summary of the integrated transport top to bottom between each station pair, and fig. 15 gives total accumulated transport across both sections. To discuss the Gulf Stream transport figures we must first decide on a definition for the 'Gulf Stream'; this is not a simple issue, and in fact Knauss (1969) suggests that this is the greatest source of discrepency among historical Gulf Stream transport calculations. One way of defining the edge is to look at where the transport per unit width changes direction. This tends to work well with the northern edge, but to the south the total transport does not diminish so quickly. To define the Sargasso Sea edge of the Gulf Stream, we look for a change in sign of the velocities somewhere rather than a change in the net transport.

We settle upon a definition which is the total net transport between stations 48-54 in the south and 60-65 in the north. This means that the width of the Gulf Stream is roughly equal at both locations and consistent with previous definitions of the Stream. The result is a Gulf Stream transport of 116 ± 2 Sv across the south section and 161 ± 4 Sv across the north. To compare with some previous estimates that only integrate down to a depth of 2000db, we figure a transport from 0-2000db of 98 ± 2 for the south and 120 ± 2 for the north.

We make a brief comparison with some historical Gulf Stream transport estimates; Table 3 lists some previous values from sections located

close to our south leg . The Richardson and Knauss result is an example of the use of discrete transport float measurements. Spatial aliasing might be a significant problem with this technique and could result in an underestimate. The Worthington (1976) numbers are averages of six historical estimates for the 0-2000db case but only two for the 0-bottom one, using a level of no motion at 2000db or the bottom. Halkin and Rossby (1985) recently performed 16 crossings at 73°W with the 'Pegasus' vertical profiler over a 2.5 year period. Their results demonstrate the variability of the transport and they arrive at a mean value slightly higher than Worthington's. Joyce et al. (1986) present Gulf Stream transports at 73°W which agree within uncertainties with the present study. Although the EN86 transects did not extend as far on the Sargasso Sea side, the Gulf Stream defined here does not include the additional length of the EN88 southern leg.

TABLE 3

Gulf Stream Transport Comparisons at 73°W

study	dates of observations	0/2000db	0/bottom
Richardson and Knauss (1971)	July, 1967	-	63 ± 5
Worthington (1976) summary	1932-1959	78 ± 7	114 ± 3
Halkin and Rossby (1985)	1980-1983	88 ± 17	-
Joyce, Wunsch, and Pierce (1986) using EN86 data	June, 1982	100 ± 6	107 ± 11
present study using EN88 data	August, 1982	98 ± 2	116 ± 2

Both the EN86 and EN88 synoptic values are above the mean offered by Worthington but well within Halkin and Rossby's range of values. Halkin and Rossby (1985) argue that Worthington's use of a level of no motion in his recalculations produces estimates that are systematically too low; their results support this. If a few more estimates were available with the same level of accuracy as the EN86 and EN88 studies, we could begin to develop a reliable mean picture to compare with the Pegasus mean. For now, our values seem to be larger than the mean estimates but within the range of variability expected for this region.

Hall (1985) calculates Gulf Stream transports using the single GUSTO current meter mooring at 68°W. From four crossings of the Stream an average transport of 103 Sv is calculated, compared to our value of 161 Sv across 71°W. Fuglister (1963) used hydrographic data and a bottom level of no motion to yield 136 Sv across 68.5°W. The Hall (1985) results required extrapolating the velocities from the current meter at 575 db to the surface, and Hall admits that the method used for this may be too conservative. Given the substantial bottom velocities across our north section, it is not surprizing that our value is also larger than Fuglister's for this region.

A downstream increase in Gulf Stream flow between our south and north sections is to be expected; this is due both to the addition of Slope Water from the north and some recirculation south of the Gulf Stream, as seen in figs. 14 and 15. The contributions from each of these effects are nearly equal; 21 Sv comes from the southwest flow north of the Stream while 24 Sv is added south of the Stream. We note a

total increase of 45 Sv, or an average downstream rate of increase of 13.9 ± 0.6 Sv/100km. Knauss (1969) studies the downstream increase in transport for the entire Gulf Stream system and predicts an average rate of 7% per 100 km; this translates to 9.7 ± 1.6 Sv/100km for this region, quite consistent with our result. Halkin and Rossby (1985) also measure this increase and report 15.4 ± 5.8 Sv/100km.

We calculate a transport for the DWBC by summing up the components of deep, high oxygen water moving southwest within the density layers 11 and 12 (Table 1). The result is 3 Sv across the south leg and 5 Sv for the north; we express our estimate as 4 ± 1 Sv. Historical estimates of the DWBC transport have varied tremendously, probably due to both time variability and differing techniques. Richardson (1977) reviews a number of historical estimates at various locations and calcalates a mean of 16 Sv but with a standard deviation of ±14 Sv. Perhaps the most reliable estimate of the mean is that of Hogg (1983), who used long term current meter records at 70°W and reported 10 Sv of 'classic' DWBC transport. Our value is below most estimates of the mean flow but certainly consistent with the apparent variability of the feature. The Cape Hatteras region is of particular interest since the Gulf Stream and the DWBC seem to cross paths here. Along our north section the DWBC is primarily found to the north of the axis of the Gulf Stream, while to the south the southwestward moving water is found on either side of the Stream. This splitting of the DWBC agrees with the observations of Richardson and Knauss (1971), who suggest that the extension of Gulf Stream flow to the bottom is connected with this separation of the DWBC

into two components. Joyce et al. (1986) quote a transport of 9 ± 3 Sv for the DWBC, closer to Hogg (1983), and present a similar DWBC structure. North of the Gulf Stream we also note a strong southwest flow of Slope Water across the north section of 23 Sv, while Joyce et al. (1986) found this to be 18 Sv.

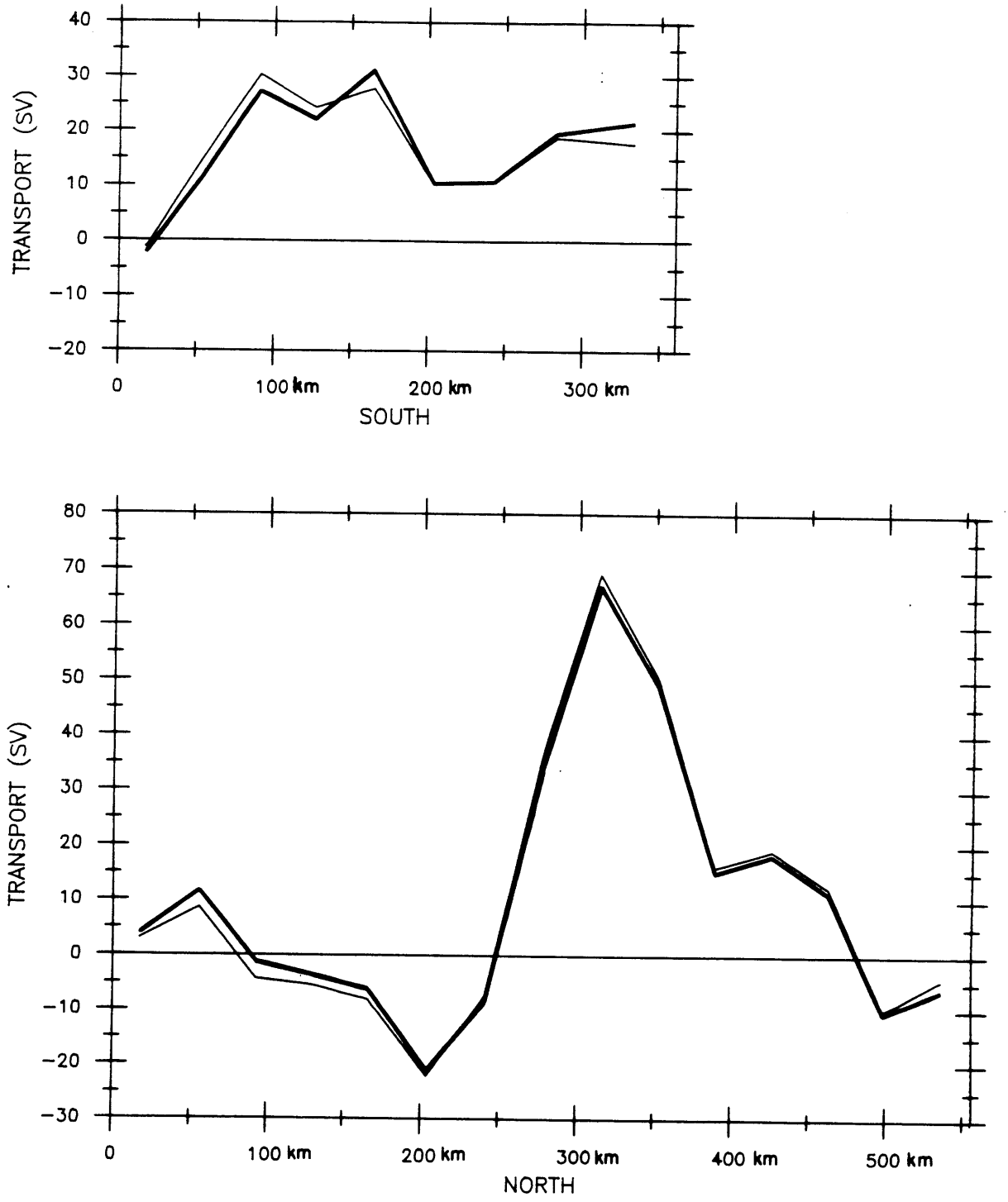

Fig. 14. Total mass transport between each station pair for the south and north sections. Heavy line is rank 36 solution; light line is rank 33. Distance scale begins at Slope Water end of sections.

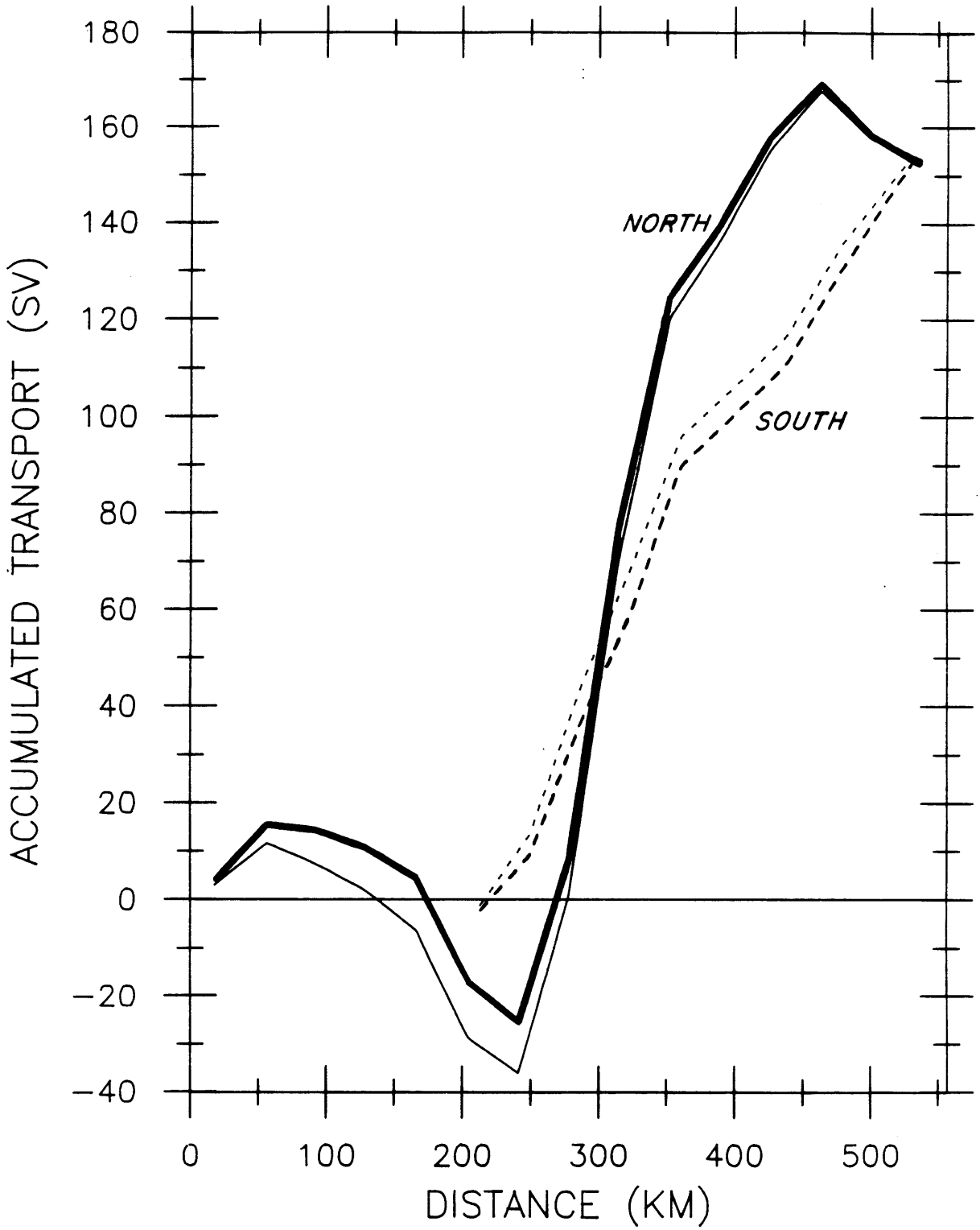

Fig. 15. Total accumulated transport across the south (dashed lines) and north (solid lines) sections. Heavier lines in either case indicate rank 36 solution; lighter lines are rank 33. Distance scale ends at Sargasso Sea corner of the region.

6. Final Remarks

We have achieved a complete description of the synoptic velocity field in the region through the combined inversion of the acoustic doppler and CTD/O_2 data. The quality of the data set and the application of the inverse techniques yield a result with smaller formal errors than any previous estimates .

The errors in the acoustic doppler velocities are dominated by the ship's navigational uncertainties; improvements in navigation techniques could greatly improve the quality of the acoustic data. More accurate LORAN or the future GPS navigation system might reduce the errors to the 1 cm/s level. This would allow meaningful direct use of the acoustic data to reference geostrophic calculations.

Since we have a region enclosed by hydrographic sections and the continental boundary, we are able to write property conservation equations appropriate for the inverse procedures introduced by Wunsch (1978). Our problem is nearly a fully determined one; in this sense it differs greatly from typical 'pure' hydrographic inversions which tend to be grossly underdetermined. The property constraints offer us additional information to refine our acoustic velocities, rather than being the only source of information in the pure case. The fact that the same procedures can be successfully applied to either underdetermined or overdetermined cases demonstrates the versatility of the technique (see Wunsch, 1985). The method allows for the extraction of any useful information out of a data set, and also allows for the incorporation of any additional data from a variety of sources. Both Joyce et al. (1986) and

the present study have demonstrated the power of the technique applied to the combination of acoustic doppler and property data.

Similar methods applied to an area with less time variability and smaller velocities could produce even greater accuracy. In this region, however, the assumption that the Gulf Stream has not varied substantially during our 4 day observation period might be a weak one; Halkin and Rossby (1985) for example have noted variations in their transport measurements of 10 Sv over the course of 7 days. This limitation implies that further efforts to improve the accuracy of our synoptic description are not warranted; we have obtained as much useful information as possible out of this 'snapshot' of a varying system.

ACKNOWLEDGEMENTS

I thank my advisor Terry Joyce and Carl Wunsch who both provided the inspiration for this work. Special thanks to Barbara Grant for her patient help with the inverse calculations. Thanks to the WHOI CTD group, Jane Dunworth, and Cleo Zani for collecting and processing data, and to Lorraine Barbour for drafting the hydrographic sections. Thanks also to many of my fellow Joint Program students for support of various kinds. Supported by National Science Foundation Grant OCE 8501176 and National Aeronautical and Space Administration Grant NAG 5-534.

REFERENCES

Beardsley, R.C. and W.C. Boicourt, On estuarine and continental-shelf circulation in the Middle Atlantic Bight, in Evolution of Physical Oceanography, Scientific Surveys in Honor of Henry Stommel, B.A. Warren and C. Wunsch, eds., The MIT Press, 198-123, 1981.

Evans, R., K. Baker, O. Brown, R. Smith, S. Hooker, D. Olson, Satellite Images of Warm Core Ring 82-B Sea Surface Temperature and a Chronological Record of Major Physical Events Affecting Ring Structure, Warm Core Rings Program Service Office, 1984. (Unpublished manuscript.)

Fuglister, F.C., Gulf Stream '60, Prog. Oceanog., 1, 265-383, 1963.

Halkin, D. and T. Rossby, The structure and transport of the Gulf Stream at 73°W, J. Phys. Oc., 15, 1439-1452, 1985.

Hall, M.M., Horizontal and Vertical Structure of Velocity, Potential Vorticity and Energy in the Gulf Stream, Ph.D. Thesis, MIT/WHOI, WHOI-85-16, 165 pp., 1985. (Unpublished manuscript.)

Hogg, N.G., A note on the deep circulation of the western North Atlantic: its nature and causes, Deep-Sea Res., 30, 945-961, 1983.

Joyce, T.M., D.S. Bitterman, Jr. and K. Prada, Shipboard acoustic profiling of upper ocean currents, Deep-Sea Res., 29, 903-913, 1982.

Joyce, T.M., C. Wunsch, and S.D. Pierce, Synoptic Gulf Stream velocity profiles through simultaneous inversion of hydrographic and acoustic doppler data, J. Geophys. Res., 91, 7573-7585, 1986.

Kennelly, M.A., The velocity structure of warm core ring 82B and associated cyclonic features, M.S. Thesis, Massachusetts Institute of Technology, WHOI-84-10, 100 pp., 1985. (Unpublished manuscript.)

Knauss, J.A., A note on the transport of the Gulf Stream, Deep-Sea Res., 16 (supplement), 117-123, 1969.

Lawson, C.L. and R.J. Hanson, Solving Least Squares Problems, Prentice-Hall, Inc., 340 pp., 1974.

Olson, D.B., R.W. Schmitt, M.A. Kennelly, and T.M. Joyce, A two-layer diagnostic model of the long term physical evolution of warm-core ring 82B, J. Geophys. Res., 90, 8813-8822, 1985.

Richardson, P.L., On the crossover between the Gulf Stream and the western boundary undercurrent, Deep-Sea Res., 24, 139-159, 1977.

Richardson, P.L. and J.A. Knauss, Gulf Stream and western boundary undercurrent observations at Cape Hatteras, Deep-Sea Res., 18, 1089-1109, 1971.

Stalcup, M.C., T.M. Joyce, R.L. Barbour, and J.A. Dunworth, Hydrographic data from warm core ring 82B, Woods Hole Oceanog. Inst. Tech. Rept. WHOI-85-29, 1985. (Unpublished manuscript.)

Volkmann, G., Deep current observations in the Western North Atlantic, Deep-Sea Res., 9, 493-500, 1962.

Worthington, L.V., On the North Atlantic Circulation, Johns Hopkins Univ. Press, 110 pp., 1976.

Wunsch, C., The general circulation of the North Atlantic west of 50°W determined from inverse methods, Rev. Geophys. and Space Phys., 16, 583-620, 1978.

Wunsch, C., Can a tracer field be inverted for velocity?, J. Phys. Oc., 11, 1521-1531, 1985.

Wunsch, C. and B. Grant, Towards the general circulation of the North Atlantic Ocean, Prog. Oceanog., 11, 1-59, 1982.

Wunsch, C., D. Hu, and B. Grant, Mass, heat, salt, and nutrient fluxes in the South Pacific Ocean, J. Phys. Oc., 13, 725-753, 1983.